International Erasmus Mundus Master in
QUATERNARY AND PREHISTORY

Morphological Correspondences between Endocasts and Calvaria: A Comparative Study across Homo and Simiiformes

Divyendu Divakar Kashyap

Supervisor/s Dr. Antoine Balzeau

Co-supervisor/s Dr. Dominique Grimaud-Hervé

Academic year 2023/2024

Contents

Acknowledgements

I would like to sincerely thank my supervisors, Dr. Antoine Balzeau and Dr. Dominique Grimaud-Hervé for helping me formulate and undertake this master's thesis.

I would like to thank Marta and Julie for helping me since the day I set foot in Europe. They helped me with academic and administrative tasks. Julie was also very kind in spending time and effort in correcting programming errors and teaching me how to use software, as was Hugo Hautavoine.

I thank Dr. Florent Détroit and Dr. Marina Mosquera for their fascinating lectures.

I would like to thank my family and numerous friends, in Europe and India for always supporting me in my endeavors and never hesitating to help.

1. Introduction

1.1 Paleoanthropology

Paleoanthropology is the study of human origins, spanning largely the last 6-8 million years of our evolution since the divergence from our last common ancestors (LCA) with chimpanzees (Amster et al., 2016; Langergraber et al., 2012). It is a comparative field of research by design, stemming from the relative paucity of samples that can be studied in comparison to other fields. Although studies on lithic assemblages, prehistoric plant and other animal remains support the field, paleoanthropology solely focuses on the direct (often fossilized) remains of hominins and sometimes hominids[1].

1.2 The Phylogenetic Relationships of Primates

Since this study, and all of paleoanthropology is situated in the larger order of primates, it is worthwhile to outline the evolutionary relationship between them. Although there is considerable debate over the origin of primates, this order seems to have originated ~80-65 Mya (Silcox, 2014) and diverged into the sub-orders Strepsirrhini and Haplorrhini ~74-65 Mya (Fleagle et al., 2017). The latter group in turn diverged into Tarsiiformes and Simiiformes (New World Monkeys and Old World Monkeys and Apes) approximately 60 Mya (Seiffert, 2012).

The earliest Platyrrhine (New World Monkey) fossil, *Perupithecus* dates to 41-36 Mya and has similarities with the North African *Talahpithecus*, suggesting an African origin and maritime dispersal to the Americas (Seiffert, 2020). Old World Monkeys ancestral to present-day macaques, baboons, and mandrills diverged from ancestral apes 30-25 Mya (Perelman et al. 2011), the latter group in turn giving rise to Hylobates and the Great Apes ~ 17 Mya (Carbone, 2014). Among the Great Apes, ancestors of Chimpanzees

[1] "Hominin" is the term used to describe a member of the lineage starting from the LCA and ending in *H. sapiens*. "Hominid' is a term used to describe all extinct and living great apes and is a superset of "hominin".

and Bonobos diverged from hominins 8-6 Mya (Pääbo, 2012) and in diverged from each other 1.5-1 Mya (Brand et al., 2022).

Although the genus *Homo* is the only extant hominin genus today, these were preceded/accompanied by the genera *Ardipithecus*, *Australopithecus*, *Paranthropus*, among others.

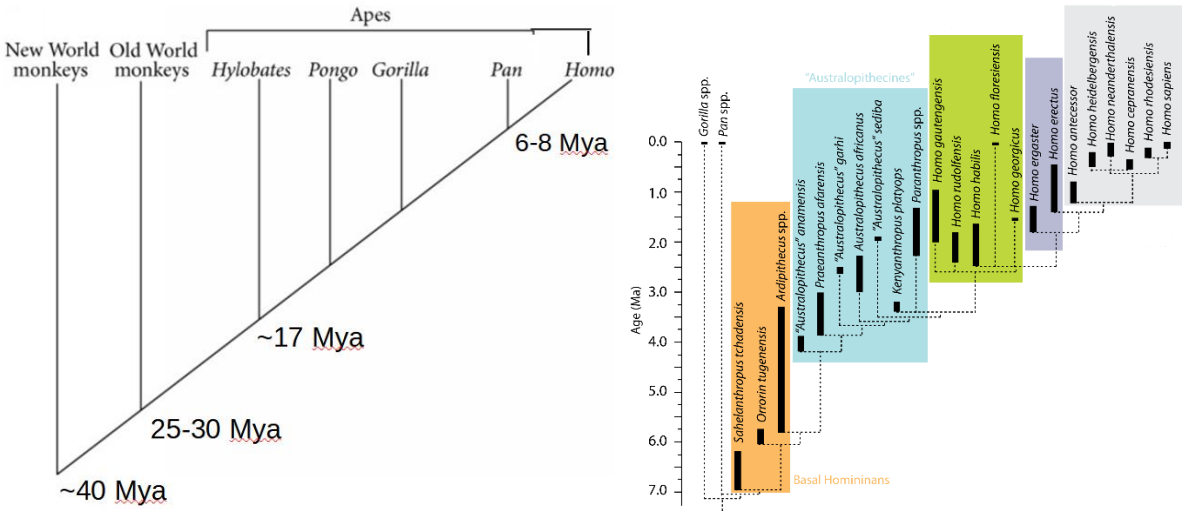

Figure 1: Phylogenies of Simiiformes (left) and Hominins (right) with estimated divergence dates (Borges et al., 2015; UMD Geology Dept., n.d.).

1.3 Paleoneurology

1.3.1 The Brain

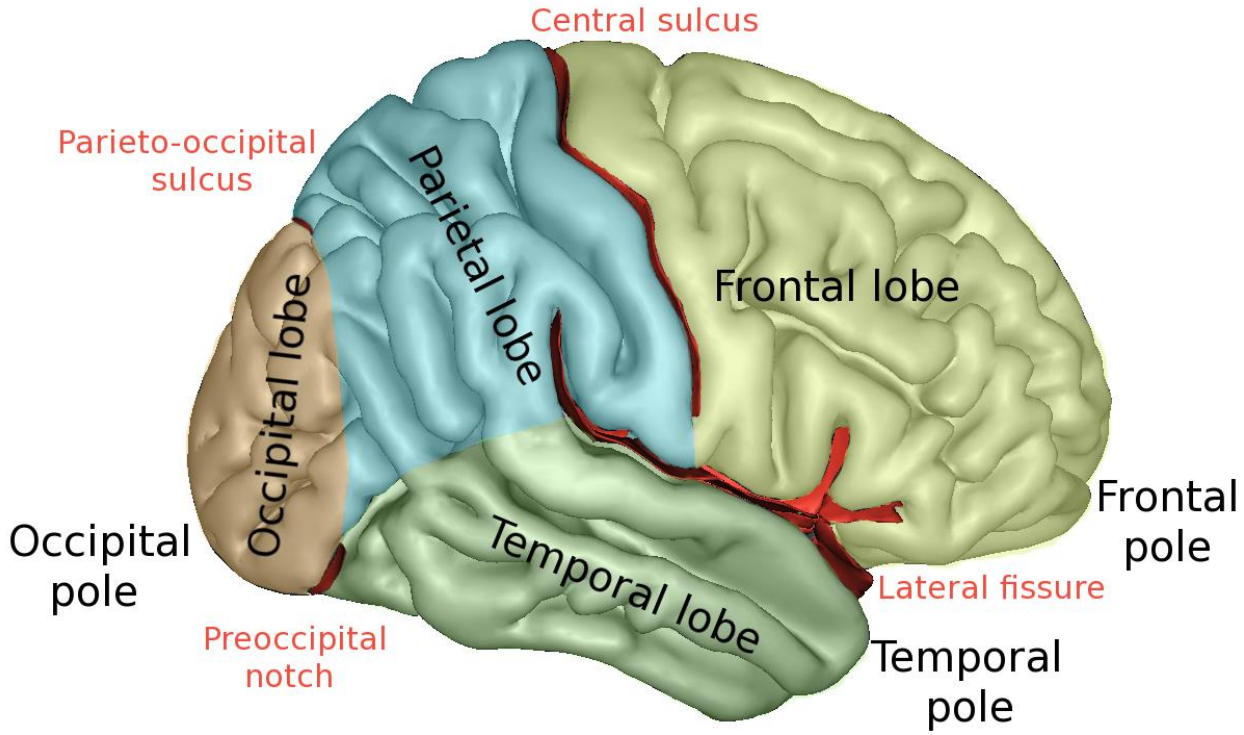

Figure 2: The human neocortex and its lobes (Wikimedea Commons, n.d.)

The human brain is a remarkable organ responsible for various involuntary functions, interpreting information from the senses, emotions, and communication, apart from cognition. It is a complex network of nerve fibers enclosed in tube-like structures called gyri. It controls every aspect of an organism's behavior and is therefore a great clue in understanding its overall biology.

In modern humans, the neocortex, making up greater than 90% of the brain, can be divided into the frontal, temporal, parietal, and occipital lobes (Willis & Haines, 2018). Each lobe (and certain areas within) in healthy human brains has a specific set of tasks and functions that it performs (Johns Hopkins Medicine,

n.d.). These are of particular importance in paleoneurology as they are the most visually perceptible areas of change across hominids.

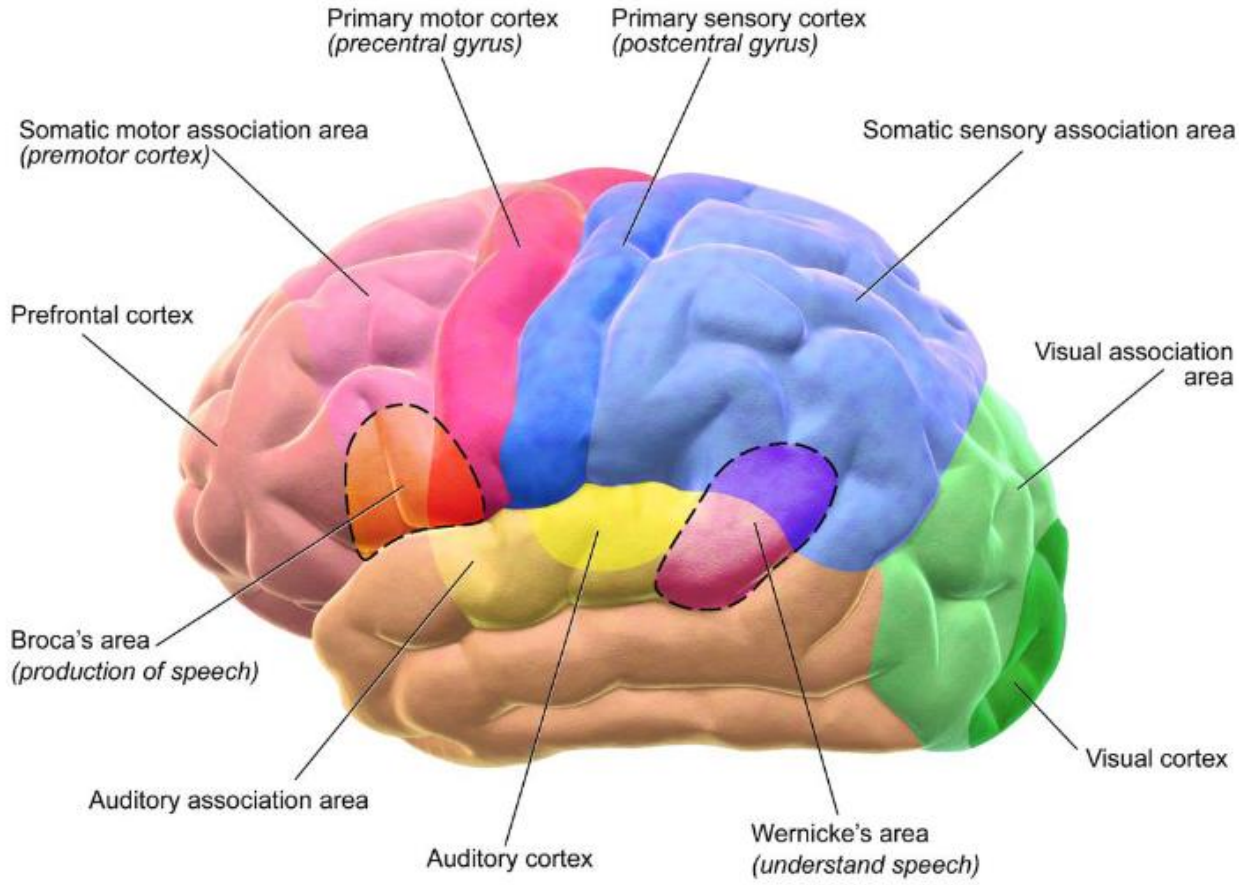

Figure 3: Areas of the human brain and their associated functions (Blausen.com staff, 2014).

Lobe	Cortical Area	Function
Frontal	Prefrontal Cortex	Problem solving, emotional regulation
	Associative Motor Complex	Complex-movement coordination
	Primary Motor Complex	Voluntary movements
	Broca's Area	Speech production
Parietal	Primary Sensory Cortex	Tactile information processing

	Somatic-Sensory Associative Area	Multi-sensorial information processing
Occipital	Visual Associative Area	Processing complex visual information
	Visual Cortex	Detection of simple visual stimuli
Temporal	Auditory Associative Area	Processing complex audial information
	Auditory Cortex	Detection of sound quality
	Wernicke's Area	Speech processing

Table 1: Areas of the modern human brain and their associated functions (Rudge & Lentz, n..d.; Jawabri & Sharma, 2023.

1.3.2 Endocasts

Unfortunately, since the brain is made up of soft tissues, it is not fossilized or preserved in the time scales concerning the present study. However, during ontogeny and the life of the organism, the brain leaves impressions of its gyri on the interior of the calvarium (Holloway et al. 2004). Endocasts are models of brains based on these patterns that can be made naturally as sediment fills up the brain case and fossilizes (Beaudet, 2017), physically by pouring molding material, or virtually through 3D imaging techniques using CT/micro-CT/MRI scanners.

Because these impressions are not through direct contact of the brain on the calvarium itself but through 3 layers of protective tissues called meninges, the extent to which key features can be discerned from calvarium has been a topic of considerable discussion (Albessard, 2018; Dumoncel et al., 2021; Labra et al., 2023). It has been suggested that the sulcal impressions on the lower part can be more accurately attributed than those on the upper part. Attempts have been made to discern positions of sulci and gyri based on skull morphology, with limited success (Kobayashi et al., 2018). The present study largely circumvents the issue by merely relying on the terminal points of the few easily identifiable sulci.

1.3.3 Previous Studies

Cross-hominin and hominid cranial comparisons have been made since the inception of paleoanthropology (Weidenreich F., 1943). Descriptions have evolved from remarks noting visual differences between fossil and modern *H. sapiens* skulls (King, 1864) to quantifying differences using geometric morphometrics (Lordkipanize et al., 2013). Fossilized hominin endocasts have also been observed quite early (Dart, 1925). Methods of quantifying shape and comparisons have included cranial capacity estimation (Dart, 1926), geometric measurements (Holloway, 1988), and sulci organizational differences (Mounier et al., 2015; Ponce de León et al., 2021).

Brain size increase has probably been the focus of the largest number of studies in the early years of paleoneurology, because of its relative ease of estimation and it being the most perceptible characteristic across hominins (Hublin et al., 2015; Bruner, 2017). However, this phenomenon might be the result of several factors at different periods of time and in different geographical locations, not necessarily equating to a greater number of neurons, but also blood vessels and glial cells (Bruner & Beaudet, 2023). It is challenging to discern these differences in the absence of the original tissues.

Qualitative studies on endocasts are not limited to sulcal identification. Detailed descriptions of the meningeal vascular system have identified continental differences in their patterns and a general reduction in sphenoparietal and petrosquamous sinuses (Grimaud-Hervé, 2004). Over the course of hominin evolution, a dominance of the anterior ramus in the middle meningeal system and increasing anastomoses on African fossils and modern *Homo sapiens* has also been observed (Grimaud-Hervé, 2004). The inferior portion of the precentral sulcus has also been shown to have moved posteriorly relative to the coronal suture over the course of the evolution of *Homo* as a consequence of frontal lobe expansion (Ponce de León et al., 2021).

Quantitative methods using morphometrics have largely relied on linear length measurements on the endocasts as these are less-controversial (Grimaud-Hervé, 2019). A few recent studies have used landmarks mostly based on points of maximum projection (Melchionna et al., 2024) and others have commented about the problems with landmarking endocasts - namely difficulties in identification especially on the parietal lobe (Pereira-Pedro & Bruner, 2018). Nevertheless, this is a relatively understudied method for analyzing endocasts and can be cautiously approached by considering the morphology of areas surrounding the trait being landmarked and a holistic understanding of brain anatomy (Pereira-Pedro & Bruner, 2018).

Few studies have considered both the endocast and calvaria morphology in the same study and tried to establish relationships between the two. An extensive study of the shape covariation between the two has been performed evaluating various areas, However, the two have not been studied in conjunction with each other in hominins. Such studies exist in the field of paleontology (Conith et al., 2023) and would be a worthwhile topic of research with the potential to inform us about not only the changes that occurred in the brain shape and organization, but its extent of influence on the surrounding skeletal structure. In addition, various regions of the crania and endocast were studied individually across several *Homo* to infer the strongest covariations being in the parietal region, and to a lesser extent, in the frontal region (Albessard, 2018).

1.4 Aims of the Present Study

The present study looks to compare both qualitatively and quantitatively, the endocasts of various specimens across *Homo* and other Simiiformes. Such a comparison has seldom been described in detail. Further, it seeks to analyze the relationship between the endocast and the calvaria through landmarks alone, to evaluate the degree of correspondence between the two. If strong enough, it could be useful in future research to gauge the position of sulci based on the more easily discernible cranial features.

2. Materials and Methods

This section provides an overview of the specimens of calvaria used in the present analysis.

2.1 Materials

A sample of 36 calvaria (and corresponding virtual endocasts), including 16 fossils were selected to showcase Late and Middle Pleistocene hominin variability particularly across Eurasia. A significant number of contemporary specimens belonging to *Homo sapiens* (7), Non-Hominin Apes (8), Cercopithecines (3), and New-World Monkeys (2) were also included to contextualize the magnitude of morphological differences. Only two of the specimens (Bonobos 26947 and 82032) seem to be juveniles.

No.	**Specimen Name**	**Species**	**Age (*Smithsonian NMNH*, n.d.)**
1.	Australia 226088	*Homo sapiens*	Contemporary
2.	Tagalog 209304		
3.	19551181		
4.	19797		
5.	19551211		
6.	19551221		
7.	196993		
8.	Cro-Magnon 1 (CM1)	*Homo sapiens*	30,000 B.P.
9.	Cro Magnon 3 (CM3)		
10.	Skhul 5		120,000 – 80,000 B.P.
11.	Ngaloba (LH 18)		120,000 B.P.
12.	La Chapelle-aux-Saints 1 (LCP)	*Homo neanderthalensis*	60,000 B.P.
13.	La Ferrassie 1 (LF-1)		70,000 – 50,000 B.P.
14.	La Quina 5 (LQ5)		65,000 B.P.
15.	Spy 10		41,000 B.P.

16.	Guattari		65,000 B.P.
17.	Saccopastore 1		130,000 - 100,000 B.P.
18.	Sambungmacan 3	*Homo erectus (sensu stricto)*	1,000,000 – 100,000 B.P.
19.	Ngangdong 7		250,000 – 70,000 B.P.
20.	Ngangdong 12		
21.	Kabwe 1 (BH)	*Homo rhodesiensis*	324,000 - 274,000 B.P.
22.	KNMER 3733	*Homo ergaster*	1,800,000 B.P.
23.	KNMER 1813	*Homo habilis*	1,900,000 B.P.
24.	Bonobo 888	*Pan paniscus* (Bonobo)	Contemporary
25.	Bonobo 11352		
26.	Bonobo 26947	*Pan paniscus* (Bonobo)	
27.	Bonobo 26958		
28.	Bonobo 27698		
29.	Bonobo 82032		
30.	Troglodytes-apple (Chimp)	*Pan troglodytes* (Chimpanzee)	
31.	Hylo 10042	Symphalangus syndactylus (Siamang)	
32.	Mandrill 3091	*Mandrillus sphinx* (Mandrill)	
33.	Papio 7868	*Papio hamadryas* (Baboon)	
34.	Macaca 1155	*Macaca arctoides* (Stump-tailed macaque)	
35.	Alouatta 961	*Alouatta caraya* (Howler monkeys)	
36.	Alouatta 963		

Table 2: List of specimens used in this study.

2.1.1 Spatiotemporal Distribution

The hominins were selected to cover various regions across the world – Africa, Europe, Asia, and a lone modern human from Australia. Although this sample is far from equally distributed in terms of chronology

due to being heavily constrained by the availability of well-preserved calvaria with clear sulcal patterns, it spans over 1.9 million years.

The extant bonobos, chimpanzee, mandrill, baboon, are native to Sub-Saharan Africa. The macaque and siamang are native to South and Southeast Asia, while the Howler monkeys are the only New World species, native to Central and South America.

2.2 Sample Acquisition

Virtual 3D models of the neurocrania and endocasts in the form of .ply and .stl files were used in this study. These were acquired provided by Dr. Antoine Balzeau (AB), through MNHN and Royal Belgian Institute of Natural Sciences collections, among others. 3D imaging techniques using CT/micro-CT scanners were used to produce these reconstructions. Avizo 7 (VGS, ©2015 FEI Company) was used to deduce the endocranial cavities and generate endocasts.

2.3 Descriptions of Methods

2.3.1 Geometric Morphometrics

Geometric Morphometric (GM) is a methodology used to quantify shape variation usually among analogous structures. While traditional morphometrics utilizes linear and curvilinear measurements of absolute lengths across specimens, geometric morphometrics takes advantage of the 3D space in which a virtual model can be visualized by recording the 3D coordinates of specific points (landmarks) on the models. In biology, these landmarks can be anatomical features such as intersections of cranial sutures that are shared among the taxa being studied (Type 1), points based on geometric features (Type 2), points that are both geometrically defined and depend on other Type 1 landmarks (Type 3), or points that are based off the positions of multiple landmarks (semilandmarks) (Bookstein, 1997). Once landmarks are placed, mathematical transformations and statistical techniques are utilized to process and accurately visualize variations. The techniques used for these purposes in this study are described here.

2.3.2. Generalized Procrustes Analysis

Generalized Procrustes Analysis (GPA) is a statistical method used in multivariate analysis and data alignment. It is often used in shape analysis but can also be applied to other types of data. In GPA, multiple sets of data, often representing different shapes or configurations, are aligned to a common coordinate system. This is achieved by scaling, rotating, and translating the landmark sets such that the sum of squared differences between corresponding points across all specimens is minimized (Slice, 2005). GPA has been used in this study to minimize the influence of variation in the overall size and thickness of calvaria and that of the scanned 3-D models itself (because of differing reference scales) on the comparative study. The GPA-transformed coordinates of the landmarks are solely based on the variation in shape of the calvaria and are hence a more accurate measure of inter-species variability. These transformed landmarks can be directly compared, or measurements can be taken to highlight differences.

However, because there are usually at least 10, and sometimes much more landmarks and semilandmarks, it can be challenging to visualize variations between each landmark across specimens. For this reason, a technique called Principal Component Analysis can be used.

2.3.3. Principal Component Analysis

Principal Component Analysis (PCA) is a statistical technique used to simplify complex data, visualize high-dimensional data, and identify underlying patterns in data. PCA is used to identify patterns and relationships in a dataset by transforming the original data into a set of linearly uncorrelated variables called principal components. Reduction in the number of variables in a dataset while retaining as much of the original variation as possible is achieved by identifying the principal components that explain the most variance in the data. The first two principal components are the directions of greatest variance in the data and are hence primarily used in the plot. In the present study, the GPA-transformed coordinates of landmarks were used in

PCA to assess the greatest inter-species variation among various hominins and simiiformes of the past and present based on the chosen landmarks.

2.4. Landmarking Scheme

13 landmarks were selected across the crania such that they provide comprehensive information on skull shape and are located closest to endocranial landmarks. These landmarks are located on the following anatomical points.

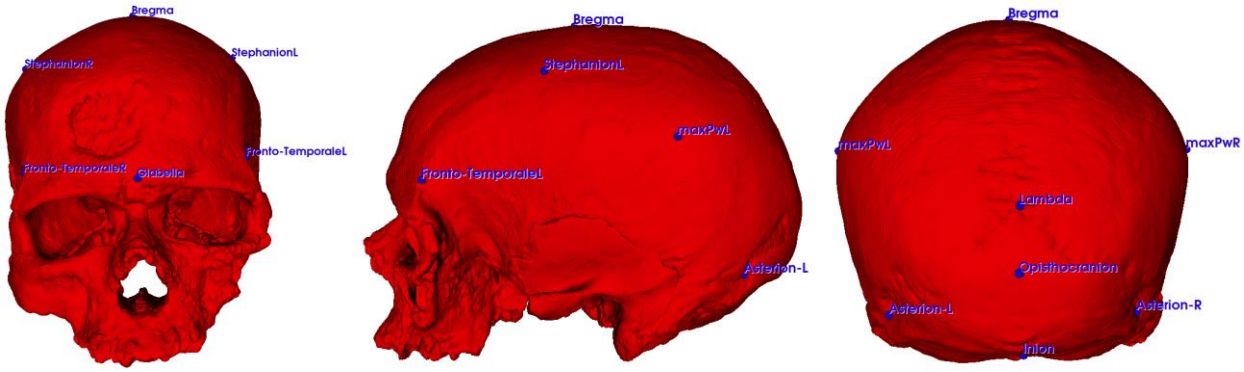

Figure 4: Cranial landmarks used in this study (norma frontalis, lateralis, and occipitalis respectively).

N.	Landmark	**Description** (Caple & Stephan, 2015)
1.	Glabella	The most projecting anterior median point on lower edge of the frontal bone, on the brow ridge, between the superciliary arches and above the nasal root.
2.	Fronto-temporale-Left	The most anterior and medial point of the inferior temporal line, on the zygomatic process of the frontal bone.
3.	Fronto-temporale-Right	
4.	Stephanion-Left	The meeting points of coronal suture with the superior temporal line.
5.	Stephanion-Right	
6.	Bregma	The meeting point of sagittal and coronal sutures.
7.	Lambda	The point at which the two legs of the lambdoid suture and sagittal suture meet.

8.	Maximum Parietal Width-Left (maxPwL)	The lateral most points on the parietal bones.
9.	Maximum Parietal Width-Right (maxPwR)	
10.	Opisthocranion	The posterior-most median point of the occipital bone, instrumentally determined as the greatest chord length from glabella.
11.	Inion	The median point between the apices of the superior nuchal lines at the base of the external occipital protuberance.
12.	Asterion-Left	The points located on the intersection of the parietal, temporal, and occipital bones.
13.	Asterion-Right	

Table 3: List of cranial landmarks used in the study.

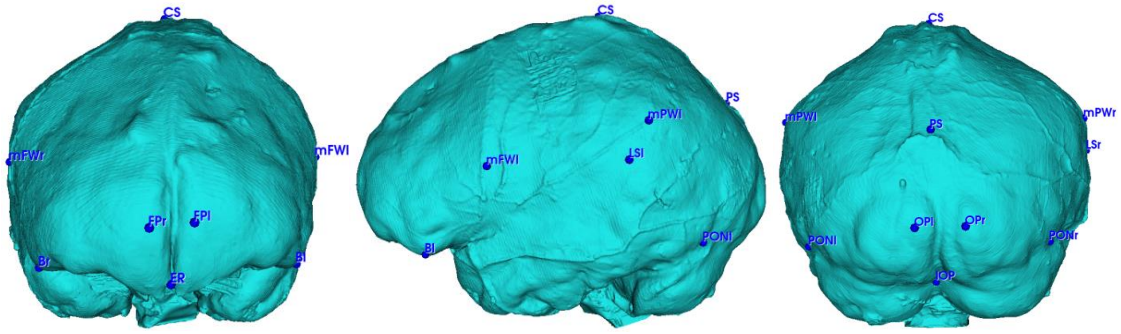

Figure 5: Endocranial landmarks used in this study (norma frontalis, lateralis, and occipitalis respectively).

18 endocranial landmarks were selected on the frontal, parietal, and temporal lobes with the help of AB. All 31 landmarks are either of Type 1 or Type 2. A combination of both points of maximum protrusion and those representing the terminal points of sulci were used in order to cover most of the endocast while only using qualitative features that were visually clear.

N.	**Landmark**	**Description** (Bruner et al., 2018)
1.	Encephalic rostrum (ER)	The medio-inferior most point on the frontal lobe.

2.	Left Frontal Pole (FPl)	Anterior most point on the left side of frontal pole.
3.	Right Frontal Pole (FPr)	Anterior most point on the right side of frontal pole.
4.	Broca's cap (Bl)	Inferior-most point of the Broca's cap.
5.	Br	The point analogous to Bl on the right side.
6.	CS	Intersection of the central sulcus with inter-hemispheric fissure.
7.	LSl	Posterior limit of the Lateral sulcus (left).
8.	LSr	Posterior limit of the Lateral sulcus (right).
9.	mFWl	Maximum frontal lobe width (left).
10.	mFWr	Maximum frontal lobe width (right).
11.	mPWl	Maximum parietal lobe width (left).
12.	mPWr	Maximum parietal lobe width (right).
13.	Preoccipital notch left (PONl)	Intersection of the Parietooccipital and Calcarine sulci (left).
14.	Preoccipital notch right (PONr)	Intersection of the Parieto-occipital and Calcarine sulci (right).
15.	PS	Central point of Parieto-occipital sulcus.
16.	Occipital Pole left (OPl)	Posterior-most point on the left side of the occipital lobe.
17.	Occipital Pole right (OPr)	Posterior-most point on the right side of the occipital lobe.
18.	Internal Occipital Protuberance (IOP)	Anterior-most point in the sagittal plane, below the occipital protuberance

Table 4: List of landmarks on the endocast used in the study.

These were placed using 3D Slicer (v 5.6.1) by the author and verified for each model by AB.

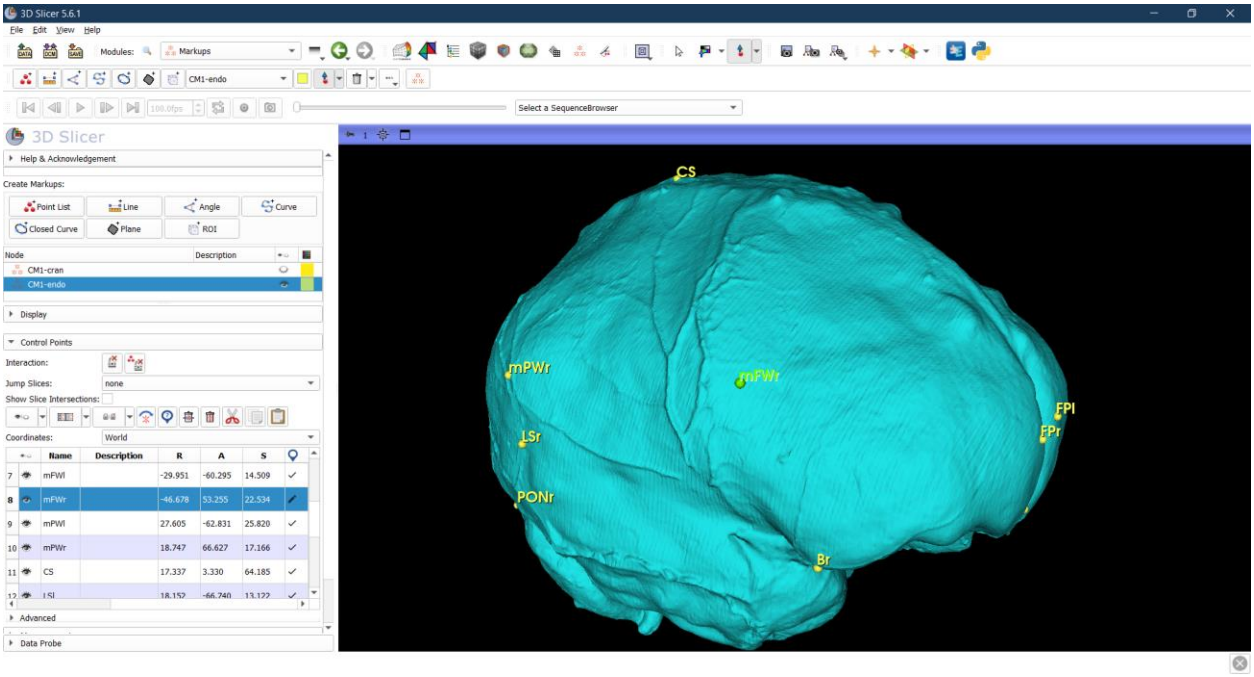

Figure 6: Placing landmarks using 3D Slicer.

These landmarks were then exported into .fcsv (Fiducial Comma Separated Values) files for analysis using R Studio.

2.5 Data Analysis

R Studio (2024.04.1+748) was used to process the .fcsv landmark files and use their coordinates in GPA and PCA. It was also used to calculate the distance between landmarks.

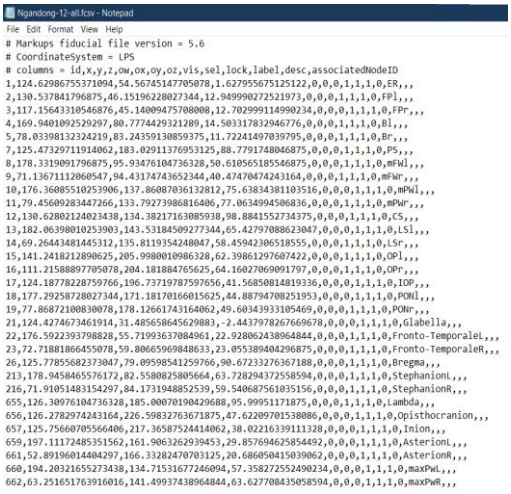

Figure 7: Exported landmark file

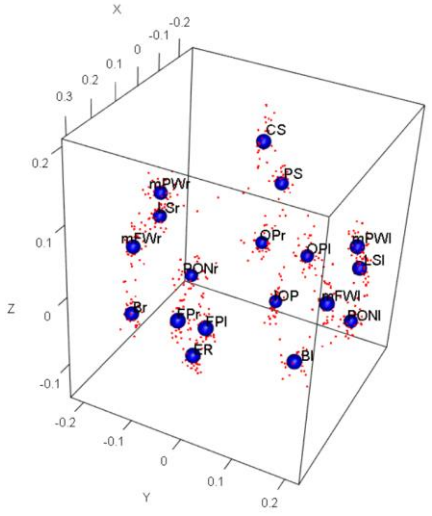

Figure 8: Visualizing GPA transformed landmarks.

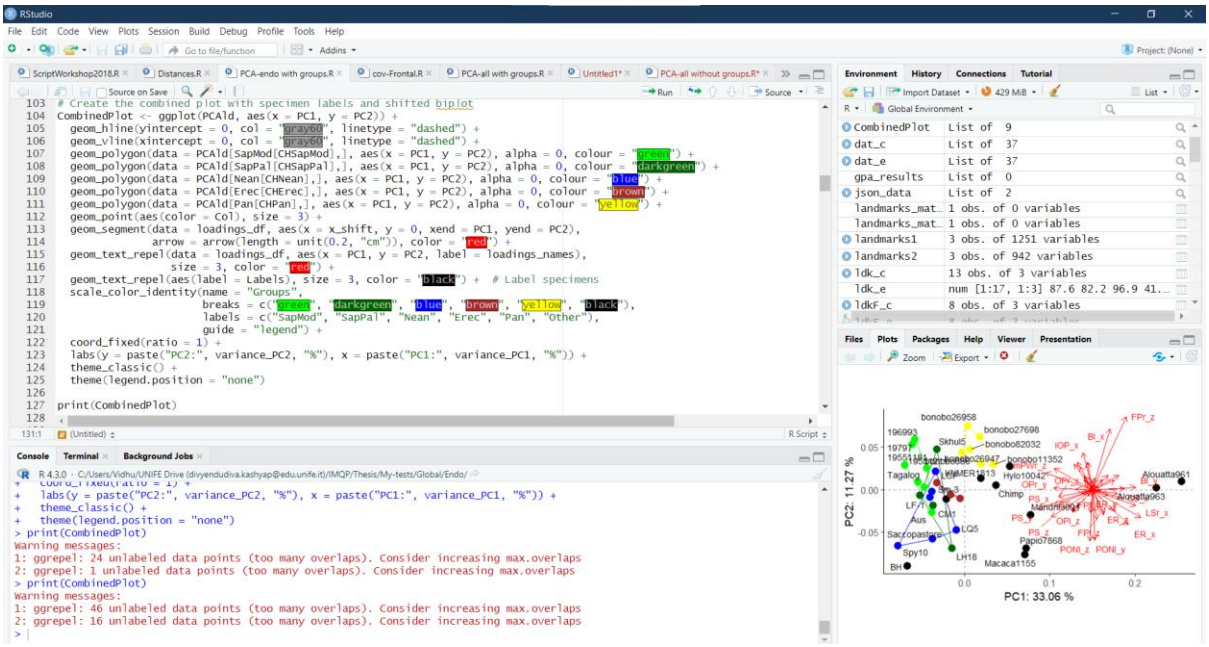

Figure 9: R Studio workspace - PCA.

3D Slicer was also used to visualize the morphing of models into GPA transformed coordinates along PCs.

3. Results

3.1 Descriptions of Specimens

A brief description of all fossil endocasts and associated crania will be given in this section, along with one example for every extant species.

3.1.1 *Homo sapiens* (Contemporary)

The example of the Tagalog specimen from Philippines is taken to represent contemporary *H. sapiens* as it is the best quality specimen in this group.

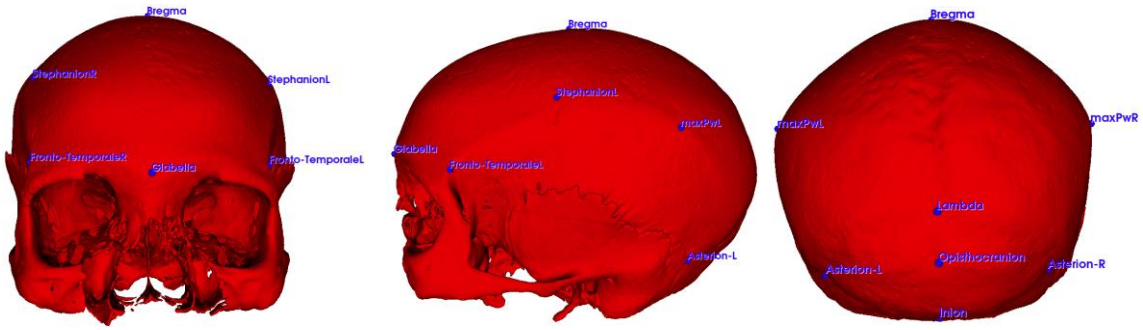

Figure 10: Figure 10: Anterior, Lateral (L), Posterior, and Superior views of the Tagalog cranium (in red).

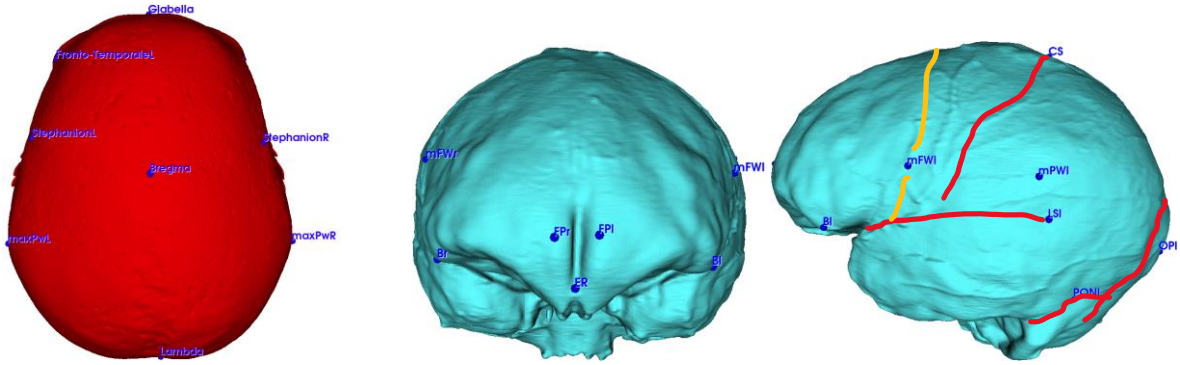

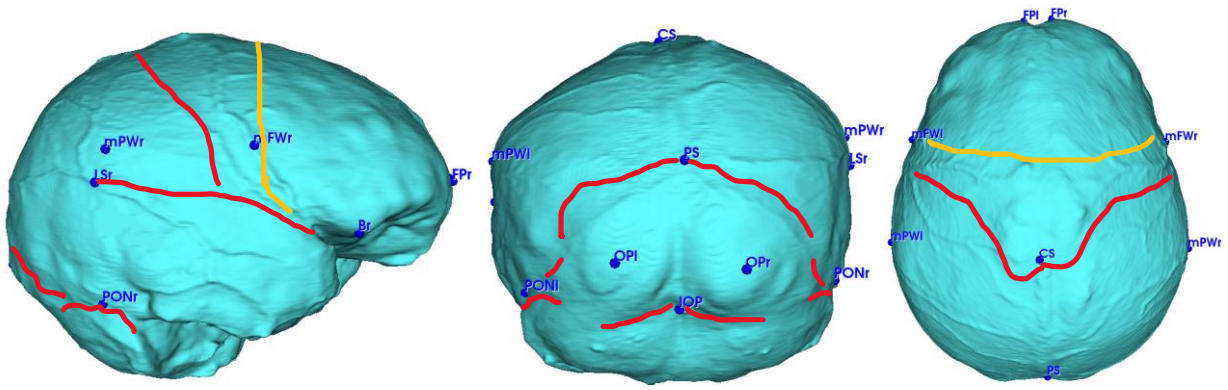

Figure 11: Anterior, Lateral (L), Lateral (R), Posterior, and Superior views of the endocast (in cyan) with the major sulci (in red) and the coronal suture (in yellow).

The cranium is typical of *H. sapiens* with a high, rounded cranial vault, elevated frontal bone, no post-orbital constriction, wide parietal bones, and a rounded occipital bone. The endocast has a left frontal/right occipital petalia, with a rightward drainage of the sinus confluence. The anterior ramus of the middle meningeal vessel seems most dominant. The terminal point of the lateral sulci on both sides are located close to the maximum parietal width.

3.1.2 *Homo sapiens* (Late Pleistocene)

3.1.2.1. Cro-Magnon 1

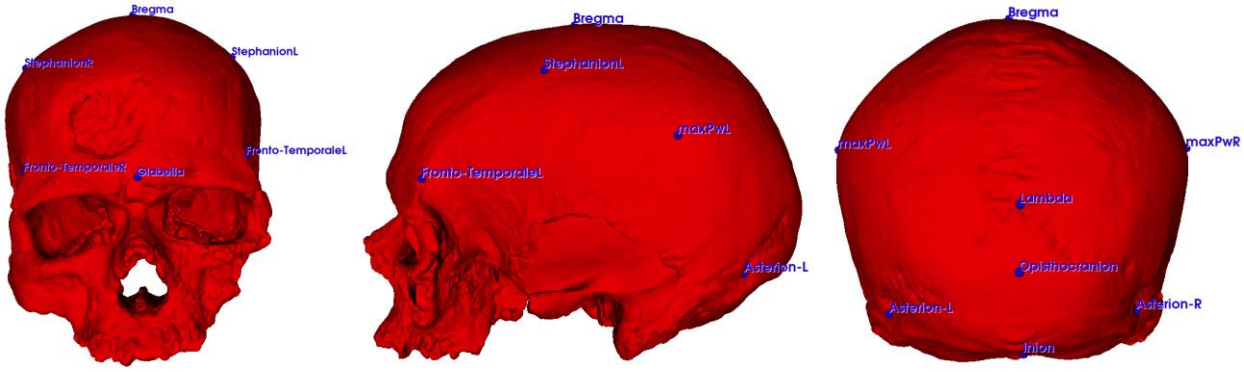

Figure 12: Anterior, Lateral (L), Posterior, and Superior views of the Tagalog cranium (in red).

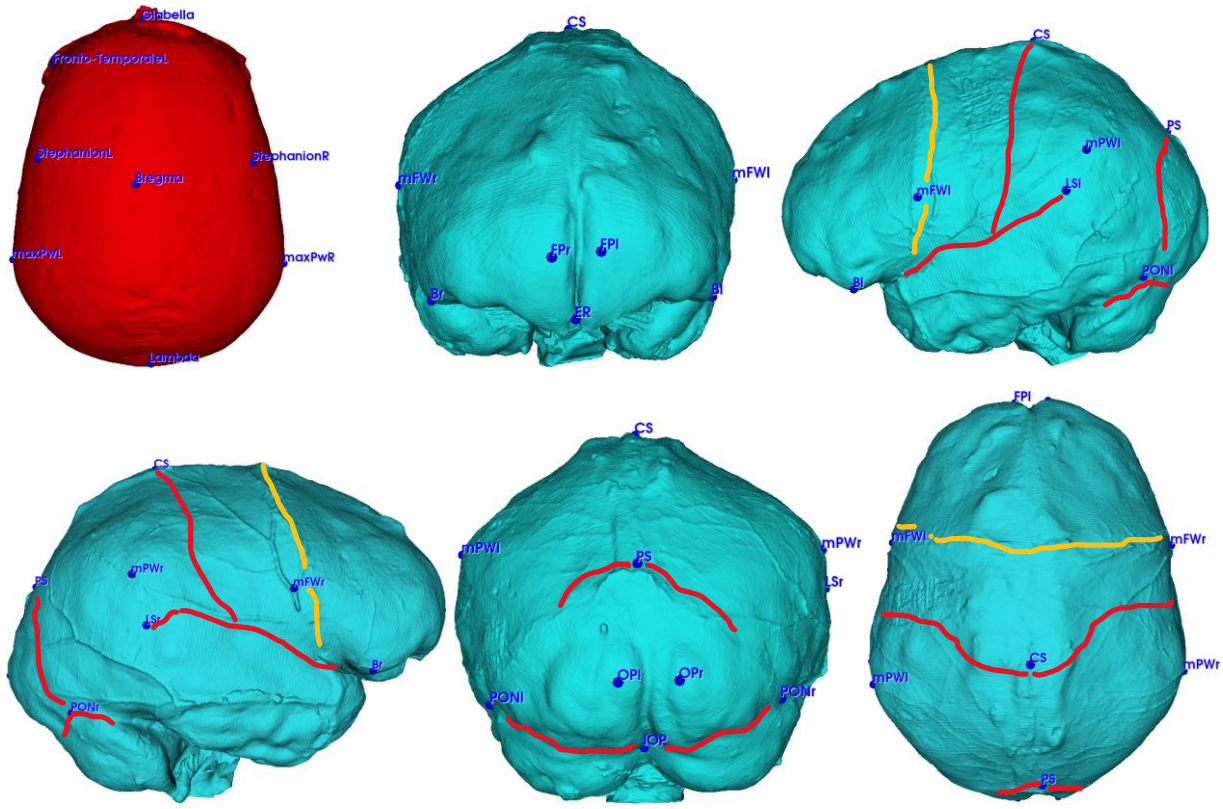

Figure 13: Anterior, Lateral (L), Lateral (R), Posterior, and Superior views of the endocast (in cyan) with the major sulci (in red) and the coronal suture (in yellow).

Cro-Magnon 1 is a relatively well-preserved skull, famous for its pathology on the right side of the frontal squama. Its overall shape is similar to that of modern humans, but certain features such as the supra-orbital torus, and the angular torus are more robust. Apart from the frontal, parietal, and occipital lobes, the temporal lobe and cerebellum are also preserved. Sulcal impressions have good visibility and are similar in form and position to those of the modern humans. Only the region immediately anterior to the left central sulci has an irregular surface due to the breccia (Balzeau et al., 2012).

The sinus confluence deviates to the right, while the anterior ramus of the middle meningeal system is the most dominant branch, running close to the coronal suture and splitting off with another branch to occupy most of the parietal lobe (Balzeau et al., 2012). The endocast exhibits a relatively uncommon right frontal/left occipital petalia.

3.1.2.2. Cro-Magnon 3

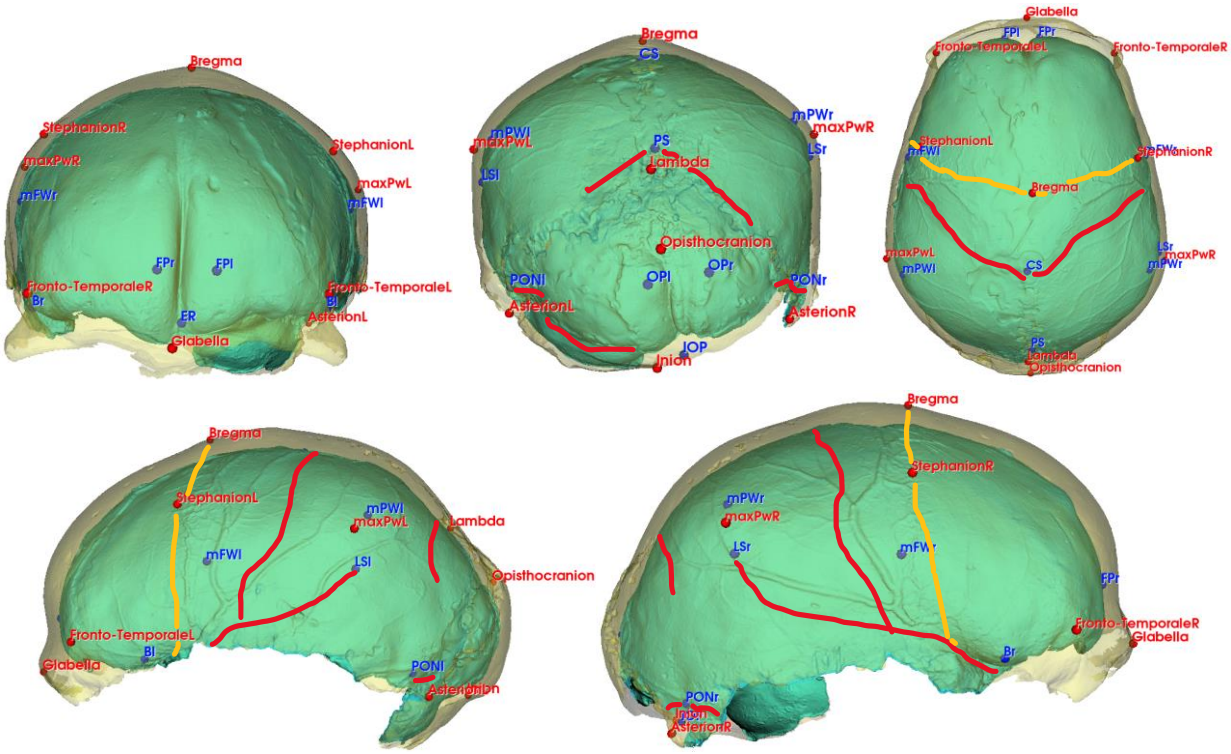

Figure 14: Anterior, Posterior, Superior, Lateral (L) and Lateral (R) views of the endocast (cyan, solid) and calvarium (yellow, solid). Endocast landmarks are shown in blue and cranial landmarks in red. Major sulci (red) and coronal suture (yellow).

Found at the same site and stratigraphic layer as the previous specimen, Cro-Magnon 3 is not as well preserved as CM1. However, it largely retains the regions relevant to the present study. Its temporal regions, right cerebellum, a large portion of the inferior right occipital regions, and smaller portions of the two on the left are missing. As a result, the Inter-Occipital Protuberance had to be intuitively placed by following the occipital-cerebellar sulci and the sinus confluence.

It shares several similarities with CM1 such as the rightward draining of the sinus confluence, a right frontal/left occipital petalia (although miniscule), and a dominant anterior ramus of the middle meningeal vessels. One difference is observed with the right lateral sulcus, which slowly rises as it progresses posteriorly, before rising sharp in its final stretch. This contrasts with what is observed in CM1, where it initially rises sharper, almost reaching the maximum parietal width, before dipping.

3.1.2.3. Skhul 5

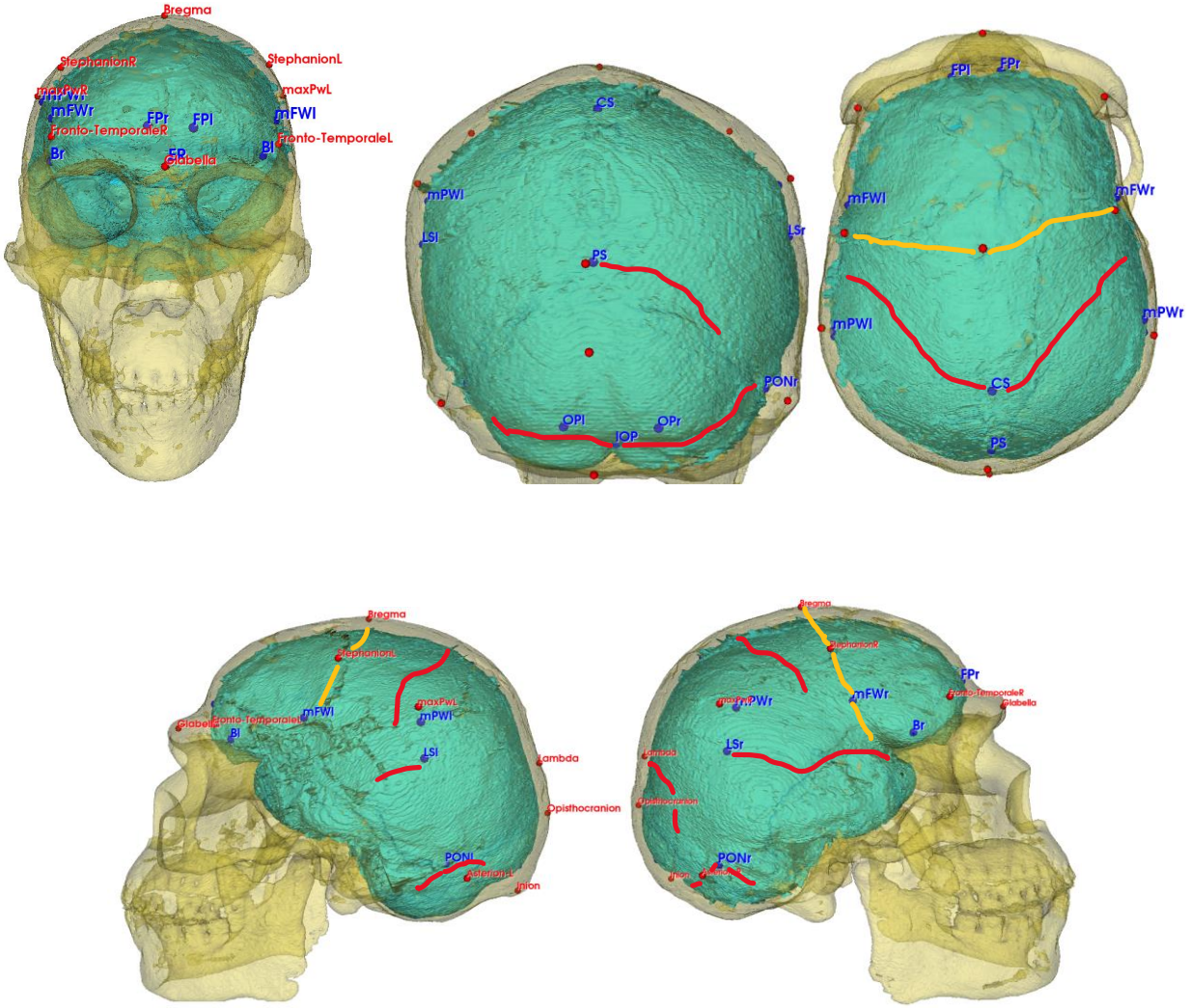

Figure 15: Anterior, Posterior, Superior, Lateral (L) and Lateral (R) views of the endocast (cyan, solid) and calvarium (yellow, solid). Endocast landmarks are shown in blue and cranial landmarks in red. Major sulci (red) and coronal suture (yellow).

Found in Mount Carmel, Israel, this is the sole specimen from West Asia used in this study. It is clearly more robust than modern humans and the Cro-Magnon specimens with its protruding supra-orbital torus and marked inferior nuchal lines. It also has a relatively receding frontal bone. Although the cranium is well-preserved, the features on the endocast are less clear, especially on the left side. The central sulcus is only discernible close to the center of the endocast, and fades as it descends. The overall shape seems similar

to the previous specimens, with a left frontal/right occipital petalia, and a rightward draining sinus confluence. There are no visible meningeal vessels.

3.1.2.4. Ngaloba (LH18)

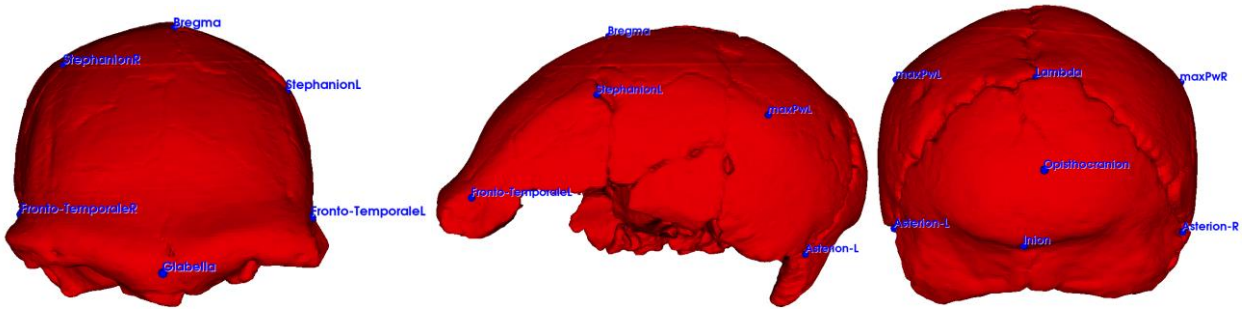

Figure 16: Anterior, Lateral (L), Posterior, and Superior views of the Tagalog cranium (in red).

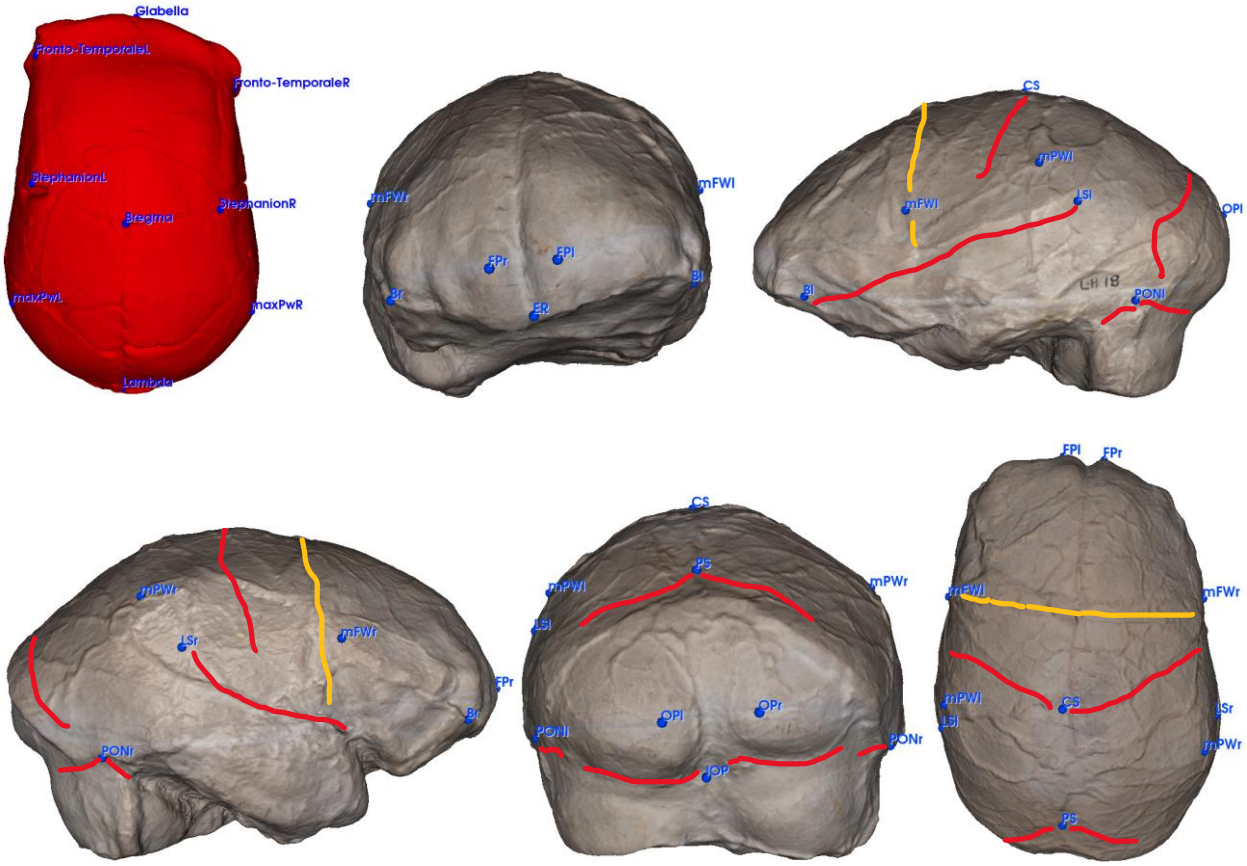

Figure 17: Anterior, Lateral (L), Lateral (R), Posterior, and Superior views of the endocast (in brown) with the major sulci (in red) and the coronal suture (in yellow).

This specimen was discovered at the site of Laetoli in Tanzania. Although complete, it is heavily distorted on its left side, as it warps to its right. This makes the positions of length-based landmarks – mFWl and mPWl less certain. Its sulcal features are also faint except in the occipital region. It exhibits a particularly strange morphology of the third frontal convolutions (Bl and Br) i.e. a minimal inferior projection, perhaps also a consequence of the distortion. Its overall shape seems much more elongated and flatter than the other *H. sapiens*. It has a minor rightward draining sinus confluence. On both sides, the anterior ramus of the middle meningeal vessels is most developed and splits into two branches close to the mFW landmarks – one oriented superiorly and the other more slanted.

3.1.3 *Homo neanderthalensis*

3.1.3.1 La Chapelle-aux-Saints 1 (LCP)

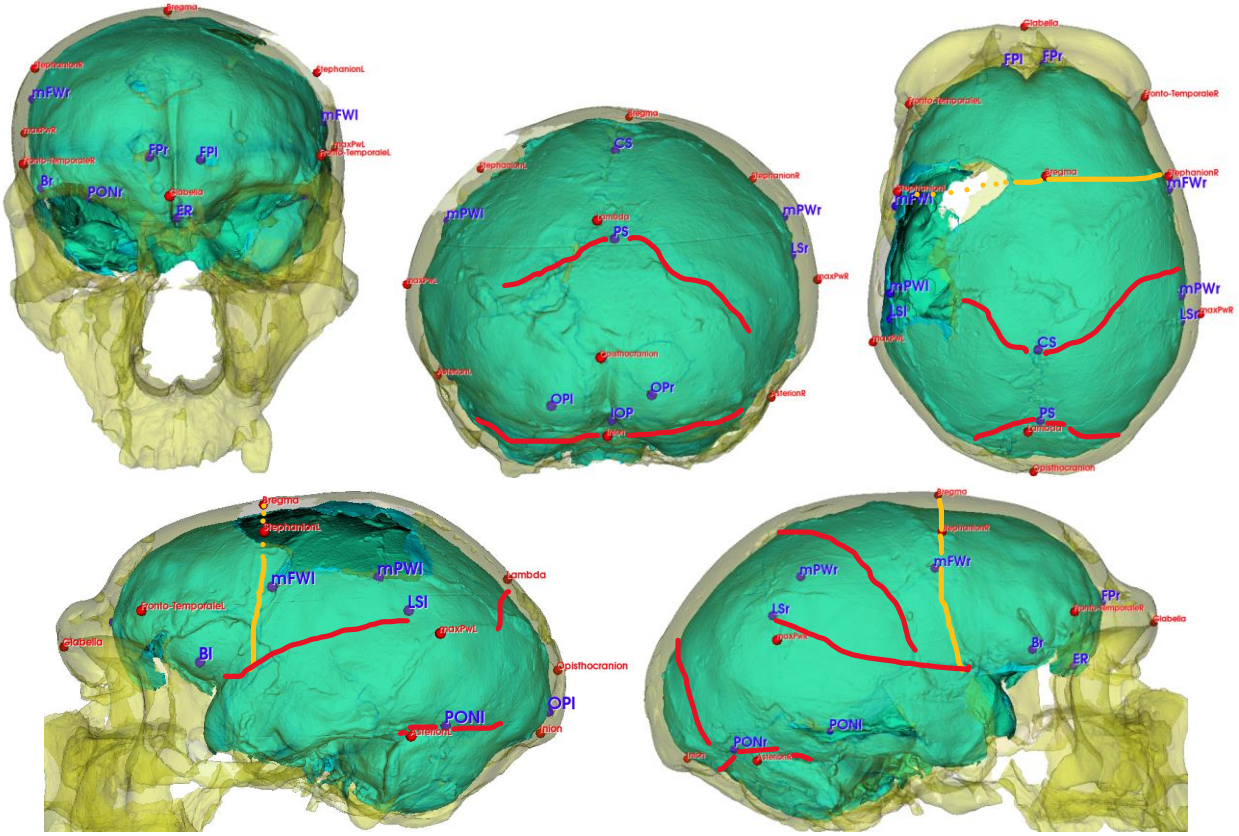

Figure 18:Anterior, Posterior, Superior, Lateral (L) and Lateral (R) views of the endocast (cyan, solid) and calvarium (yellow, solid). Endocast landmarks are shown in blue and cranial landmarks in red. Major sulci (red) and coronal suture (yellow).

Most likely belonging to a male, this individual was old at the time of his death and suffered from a joint disease (Smithsonian NMNH, n.d.). The cranium exhibits classic Neanderthal characteristics with a strong supra-orbital torus, receding forehead, and mid-face prognathism. Overall, the specimen is elongated, shorter in elevation, and widest at a lower height when compared to the *H. sapiens* specimens. A huge chunk of the left frontal and parietal regions are missing, leading to an estimated position of the Stephanion landmark based on the direction of the coronal suture and its analogue on the right side.

The overall shape of the endocast is ovoid, and it has a slight right frontal/left occipital petalia. Sulci can be identified quite clearly and with a high degree of certainty. The anterior and posterior branches of the middle meningeal vessels are equally dominant and slope diagonally posteriorly. The sinus confluence drains slightly rightward. The positions of landmarks relative to each other are not much different from those on *H. sapiens*. But there is a noticeable overall elongation and reduction in the height of the endocast.

3.1.3.2 La Ferrassie 1 (LF1)

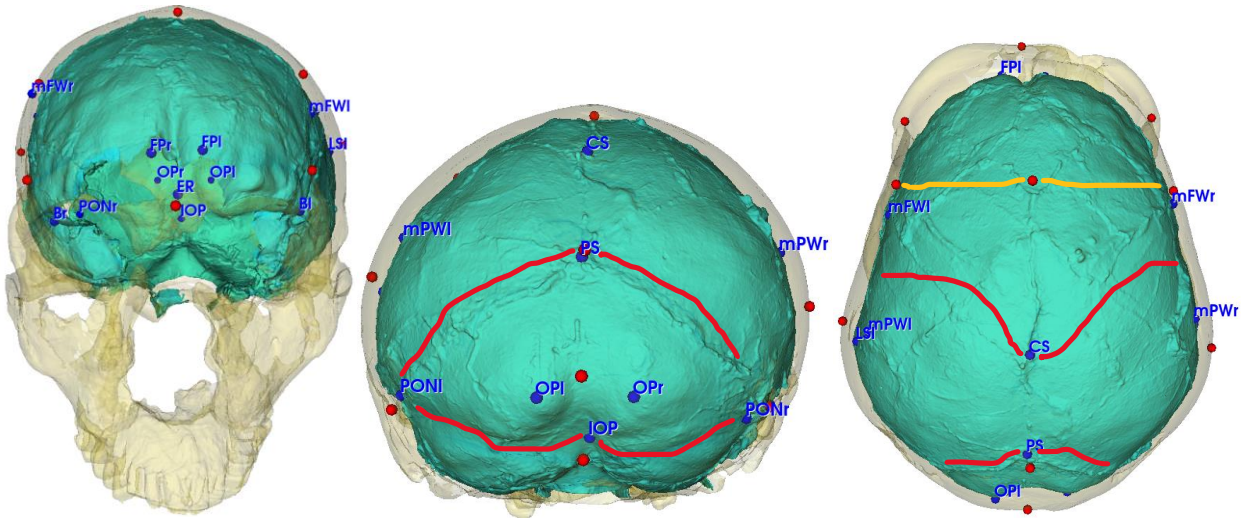

Figure 19: Anterior, Posterior, Superior, and Lateral (next page) views of the endocast (cyan, solid) and calvarium (yellow, solid). Endocast landmarks are shown in blue and cranial landmarks in red. Major sulci (red) and coronal suture (yellow).

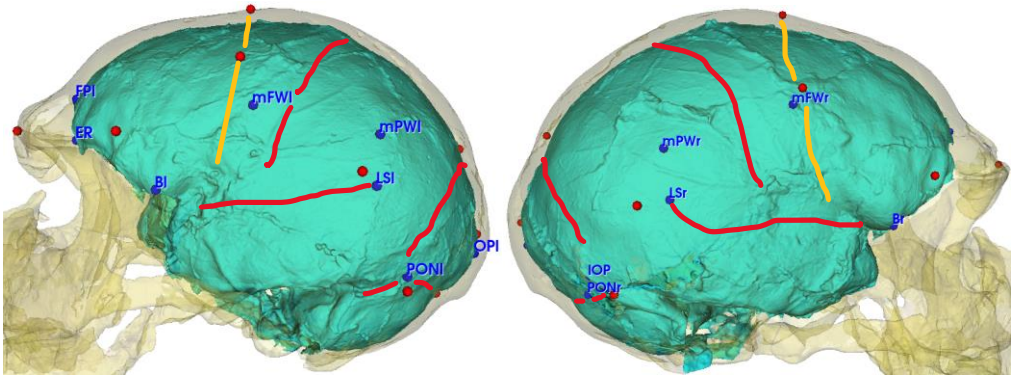

Another old male individual showing classic neanderthal traits, this specimen is known for its uniquely worn incisors, hypothesized to have been a result of manipulating objects. This specimen is missing a part of its frontal region, and therefore, the position of the encephalic rostrum and the right frontal pole had to be estimated based on the surrounding morphology and the sagittal sinus.

Overall, the endocast appears rounder than LCP, with a slight left occipital petalia. However, it is longer and shorter than the *H. sapiens* endocasts, and the inferior part of the occipital lobe slopes downward, characteristic of Neanderthals. It is interesting to note that the maximum parietal widths are slightly posterior to the posterior extent of the lateral sulci, as in the case of the mPWr of LH18. Contrary to LCP, the anterior rami of the middle meninges have an obelic branch and is more prominent than the posterior branch (Grimaud-Hervé, 2004). There is no noticeable preference for the sinus confluence drainage.

3.1.3.3 La Quina 5 (LQ5)

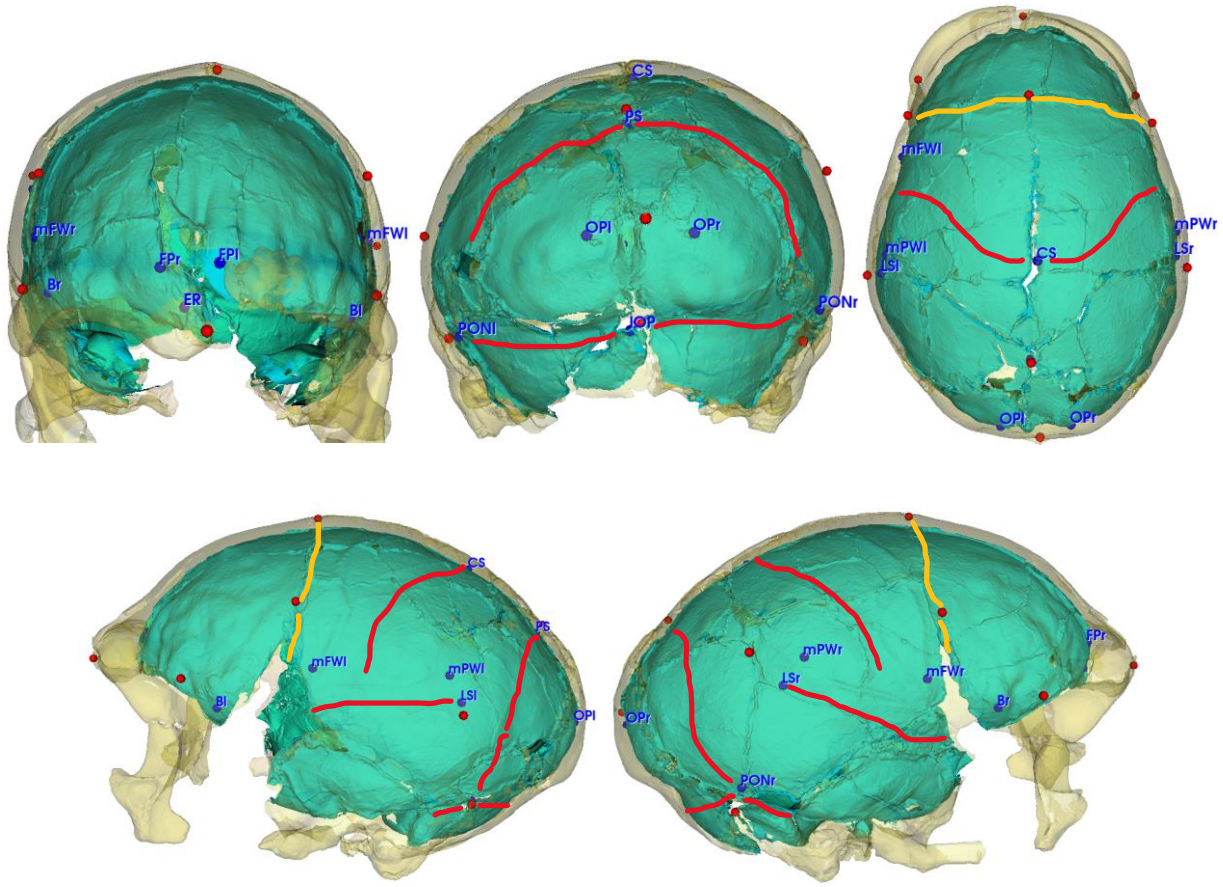

Figure 20: Anterior, Posterior, Superior, and Lateral (next page) views of the endocast (cyan, solid) and calvarium (yellow, solid). Endocast landmarks are shown in blue and cranial landmarks in red. Major sulci (red) and coronal suture (yellow).

This specimen is extremely fragmented, but the reconstruction preserves most of its key features. A part of its right frontal region, near the lobe is missing, and the region seems to be deformed, warping rightwards. It also has parts missing behind the third frontal convolutions, and close to the lambdoid suture. Its overall shape is similar to that of LCP, with a greater elongation and vertically shorter endocast than LF1. However, its middle meningeal system is like that of LF1, with a dominant anterior ramus with an obelic branch (Grimaud-Hervé, 2004). The maximum parietal widths are noticeably lower, and closer to the posterior terminus of the lateral sulcus.

3.1.3.4 Spy 10

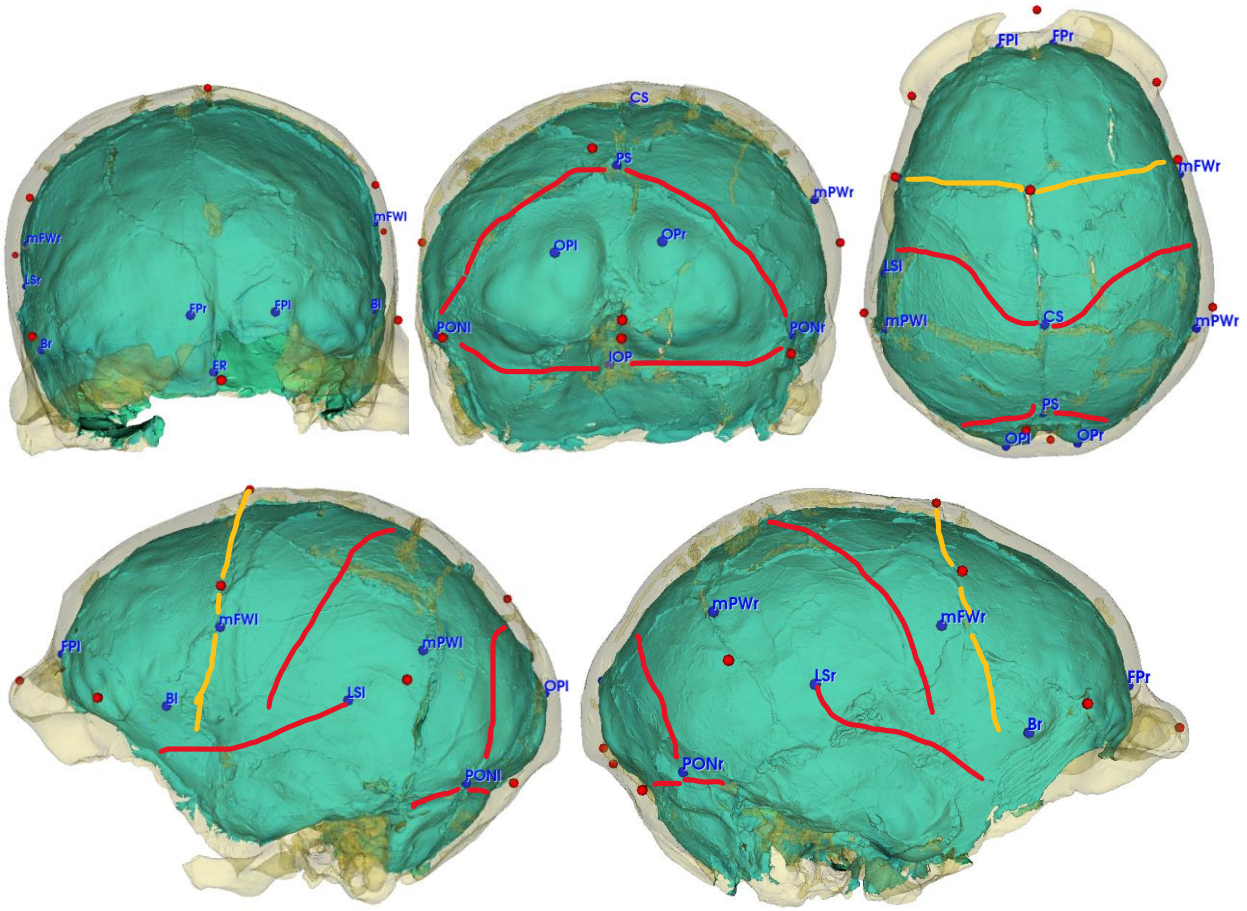

Figure 21: Anterior, Posterior, Superior, and Lateral views of the endocast (cyan, solid) and calvarium (yellow, solid). Endocast landmarks are shown in blue and cranial landmarks in red. Major sulci (red) and coronal suture (yellow).

Visually, the endocast resembles LF1, with a more rounded overall shape. The specimen is missing its left inferior frontal region, but the positions of the glabella and encephalic rostrum are not. Its parietal and occipital regions have been reconstructed and are fragmented but preserve most areas. The sulcal detection on this specimen is made with moderate certainty. It does not exhibit any significant petalias and has its maximum parietal width much more posterior than the posterior extent of the observable lateral sulci, although this probably has more to do with the LS visibility than the mPWs. There is a noticeable rightward drainage of the sinus confluence. A slight deformation in the inferio-posterior part of frontal lobe makes it difficult to discern the meningeal vessels pattern, but it seems that the obelic branch of the anterior ramus is more dominant.

3.1.3.5. Guattari

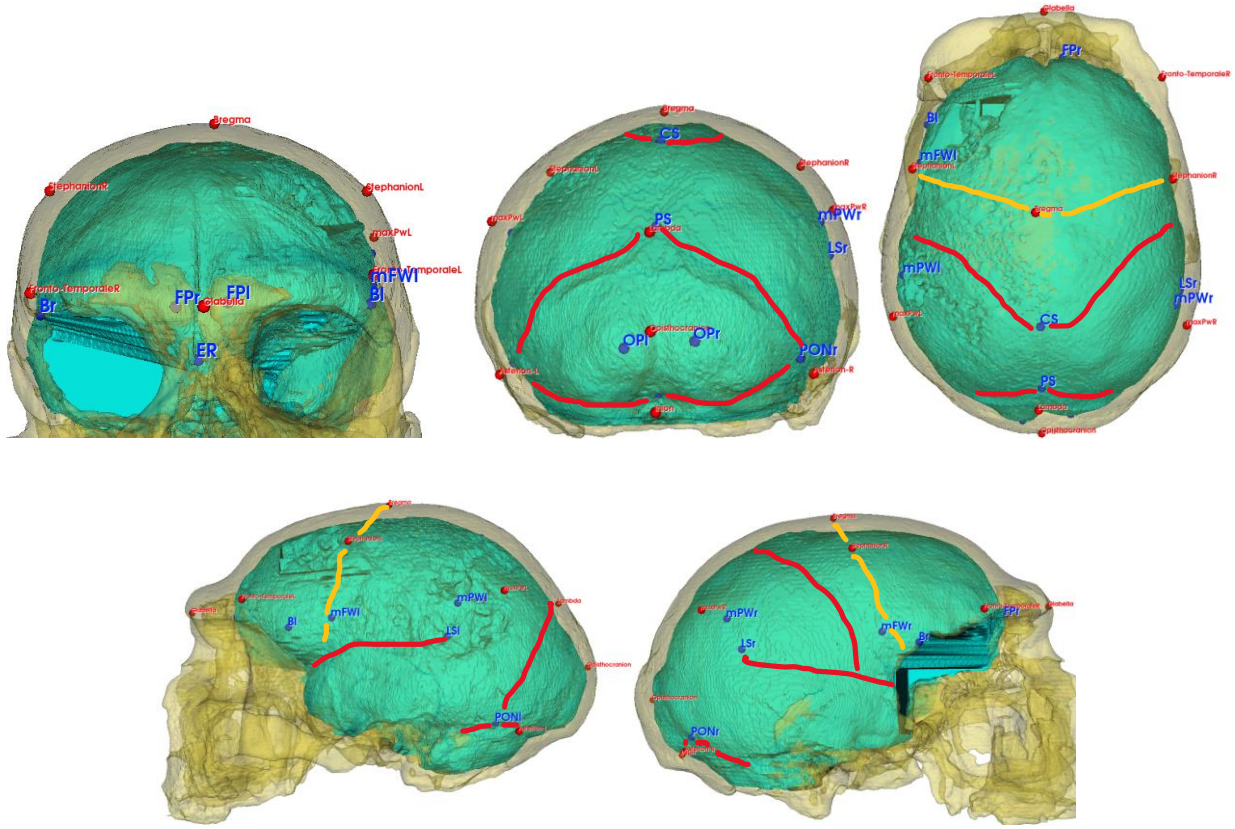

Figure 22: Anterior, Posterior, Superior, and Lateral views of the endocast (cyan, solid) and calvarium (yellow, solid). Endocast landmarks are shown in blue and cranial landmarks in red. Major sulci (red) and coronal suture (yellow).

This specimen was found in western Italy and is missing its right fronto-temporal and left fronto-parietal regions, including the left extent of the central sulcus and a part of its the third right frontal convolution. The position of CS is valid due to good preservation of the right extent of the central sulcus, but Br may or may not be positioned lower. LSl may also be located more inferiorly, but these are the most conservative positions. It exhibits a left occipital petalia, no noticeable preference for the sinus confluence drainage and no visible meningeal vessels.

3.1.3.6. Saccopastore 1

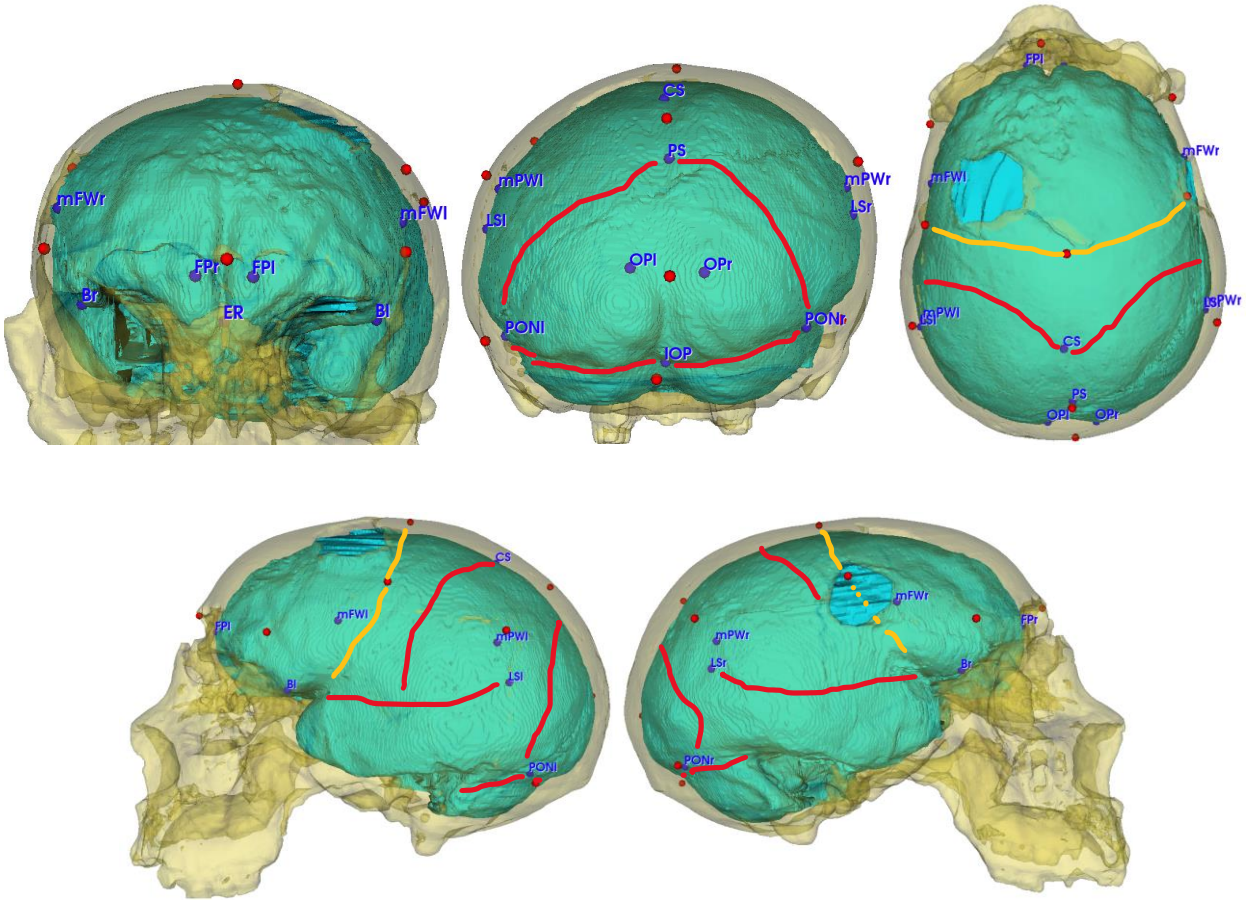

Figure 23: Anterior, Posterior, Superior, and Lateral views of the endocast (cyan, solid) and calvarium (yellow, solid). Endocast landmarks are shown in blue and cranial landmarks in red. Major sulci (red) and coronal suture (yellow).

This specimen was also recovered in Italy and is significantly older than the other specimens. While it still bears the classic Neanderthal traits, it is not as elongated as the other specimens. It is well-preserved, apart from two patches on either side of the frontal lobe. It exhibits a left occipital petalia, a rightward drainage of the sinus confluence, and no visible meningeal vessels.

3.1.4. *Homo erectus* (sensu stricto)

3.1.4.1. Sambungmacan 3

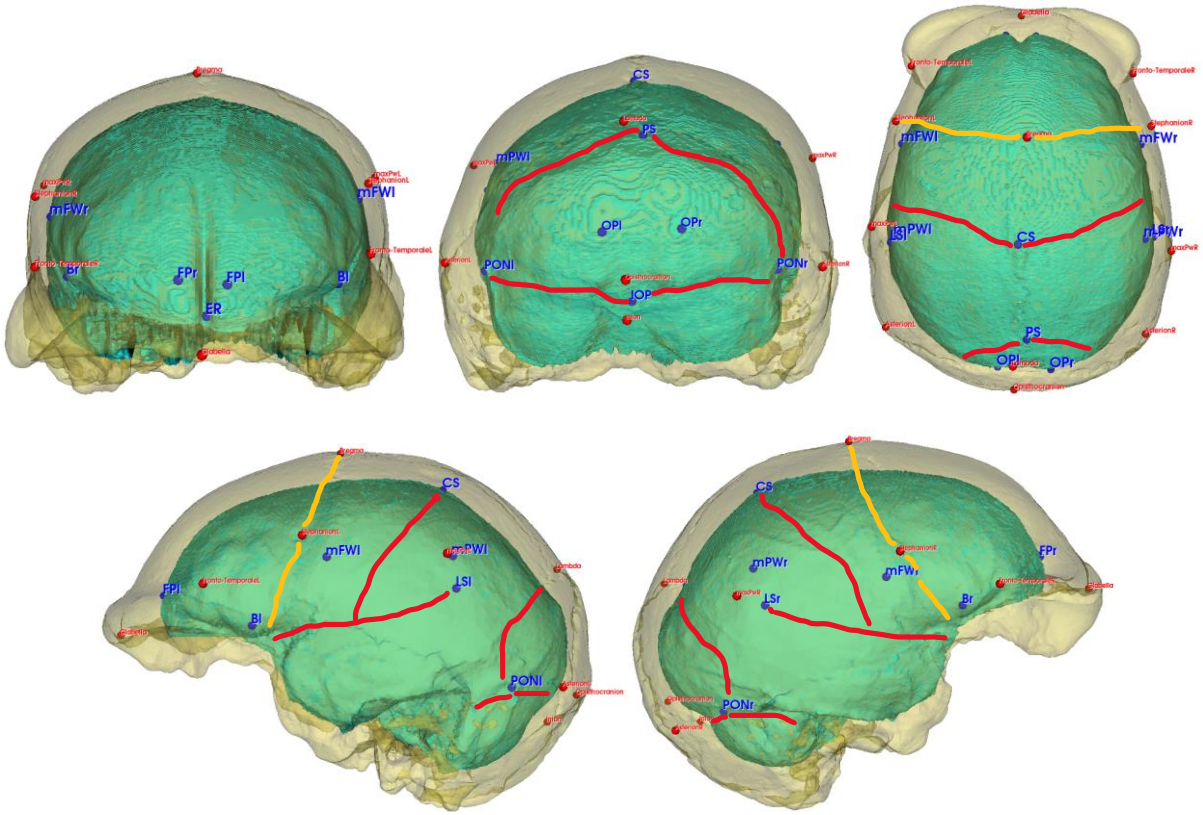

Figure 24: Anterior, Posterior, Superior, and Lateral views of the endocast (cyan, solid) and calvarium (yellow, solid). Endocast landmarks are shown in blue and cranial landmarks in red. Major sulci (red) and coronal suture (yellow).

The skull cap of this specimen is well-preserved. The main differences are a more sloping and longer frontal bone, the presence of an occipital torus, and a relatively strong post-orbital constriction. The endocast is relatively smooth with moderately low visibility of sulci. It has a left frontal/right occipital petalia, with no visible preference of sinus confluence drainage. The obelic branch of the meningeal vessels is most dominant.

3.1.4.2. Ngandong 7 (Ng7)

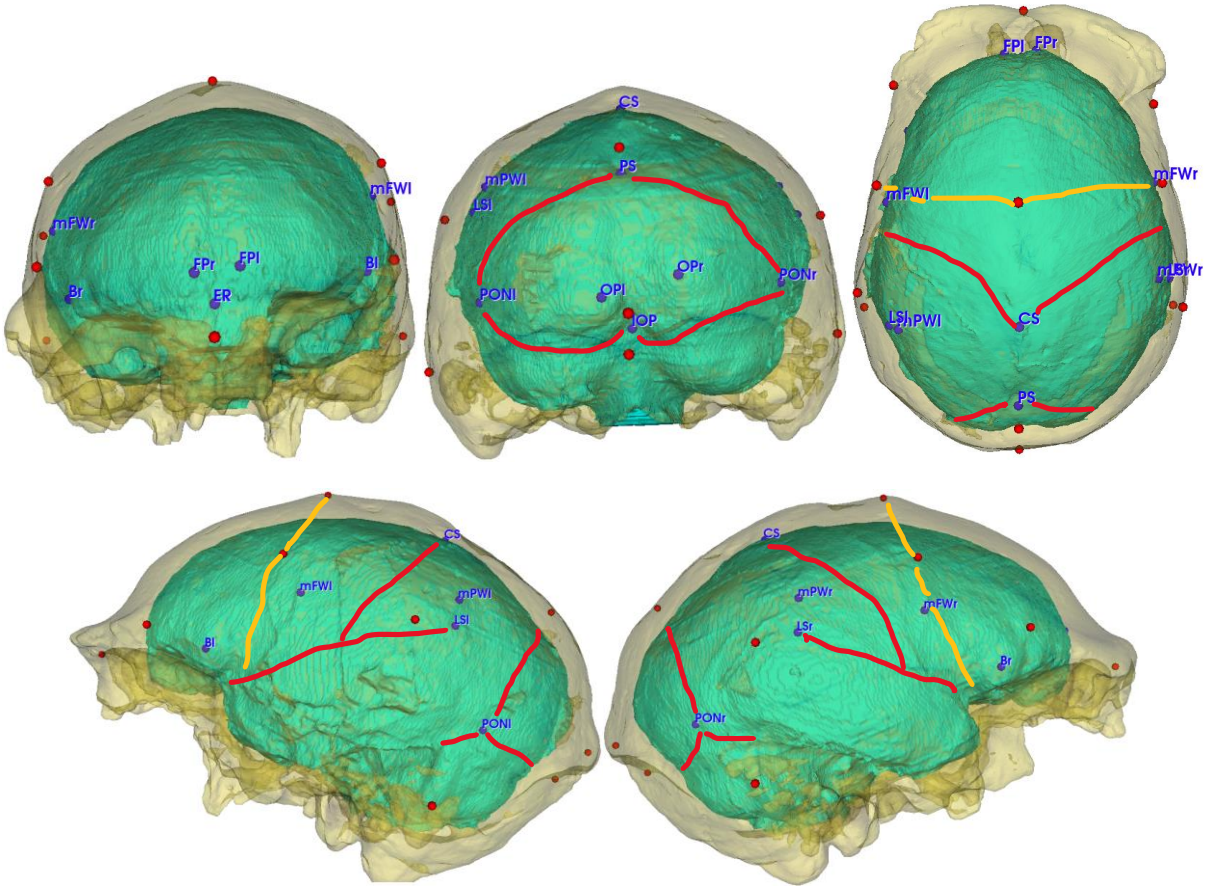

Figure 25: Anterior, Posterior, Superior, and Lateral views of the endocast (cyan, solid) and calvarium (yellow, solid). Endocast landmarks are shown in blue and cranial landmarks in red. Major sulci (red) and coronal suture (yellow).

The skull cap of Ng-7, akin to Sm-3, is well preserved but its endocast has relatively poor delineation of sulci. It has no visible petalia, preference of sinus drainage, or meninges vessels. Unlike in Sm-3, the central sulcus is not parallel to the coronal suture, but follows the pattern observed in *H. sapiens* and *H. neanderthalensis*.

3.1.4.3. Ngandong 12 (Ng12)

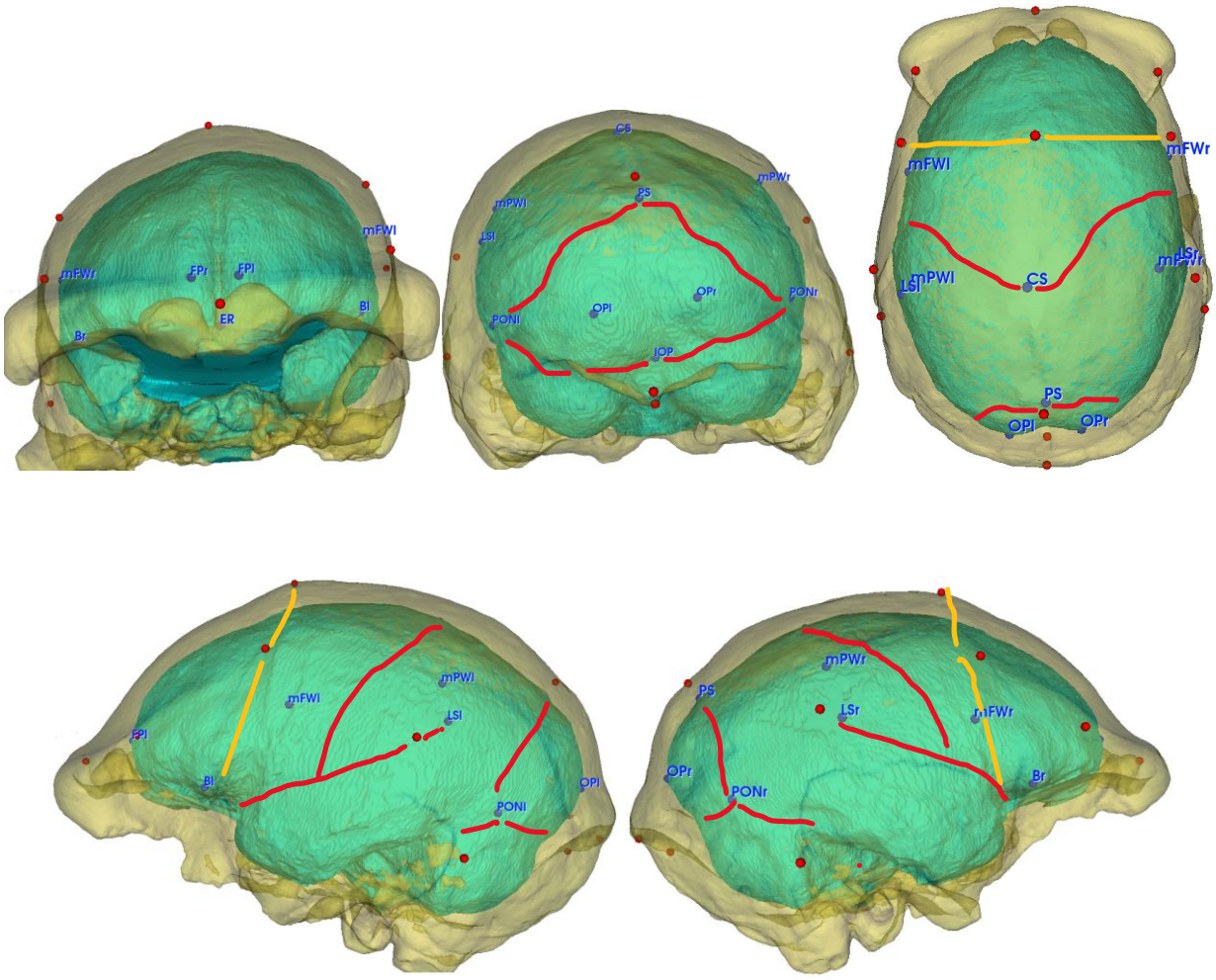

Figure 26: Anterior, Posterior, Superior, and Lateral views of the endocast (cyan, solid) and calvarium (yellow, solid). Endocast landmarks are shown in blue and cranial landmarks in red. Major sulci (red) and coronal suture (yellow).

This specimen is virtually identical to the Ng 7, as expected from crania found within the same stratigraphic layers. The state of preservation, lack of meningeal vessels, petalias, and a dominant side of sinus drainage is also the same as Ng 7. Overall, Indonesian *Homo erectus* seem less visually different from each other compared to *H. sapiens* and *H. neanderthalensis*. They also exhibit unusually large distances between Asterion and the Pre-occipital notch landmarks.

3.1.5 *Homo rhodesiensis* (Kabwe 1/Broken Hill/BH)

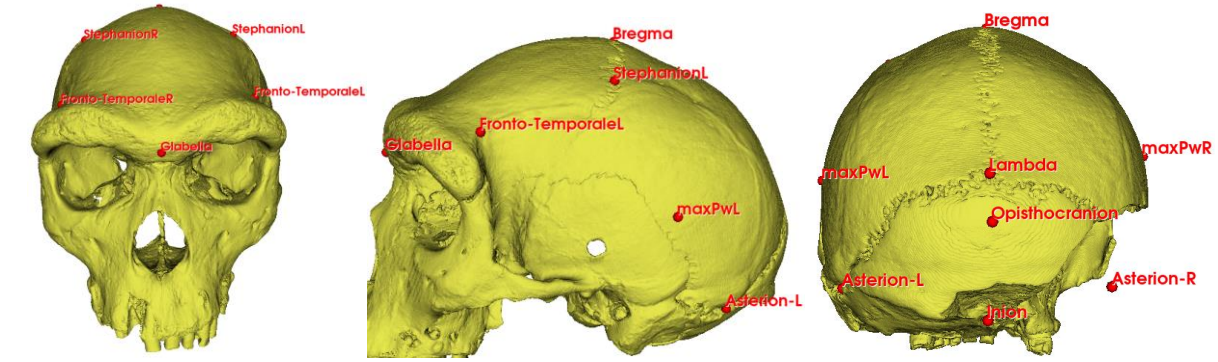

Figure 27: Anterior, Lateral (L), Posterior, and Superior views of the BH cranium (in yellow).

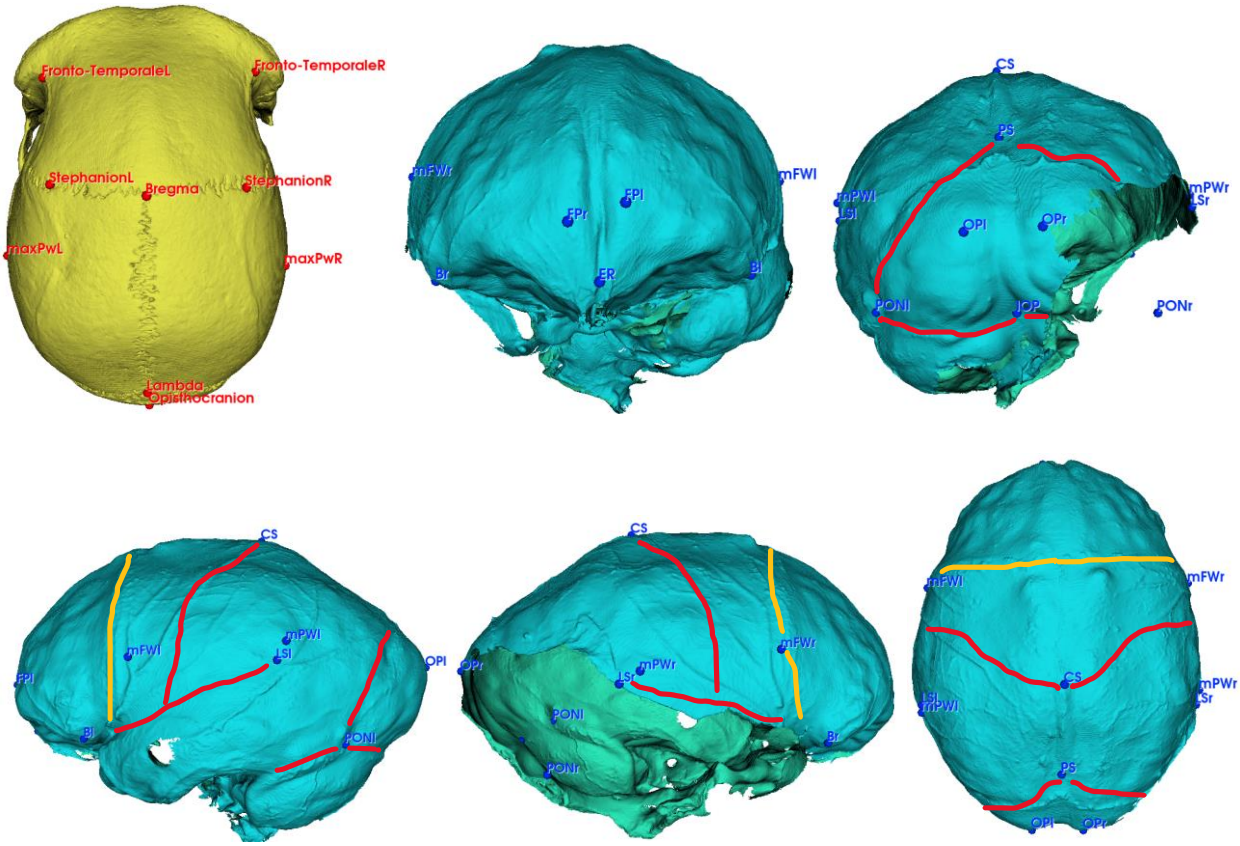

Figure 28: Anterior, Lateral (L), Posterior, and Superior views of the BH endocast (in cyan) with major sulci (in red) and the coronal suture (in yellow).

The BH cranium has been the subject of great debate with its phylogenetic position. It is missing a huge chunk of the right side of its occipital, cerebellar, temporal lobes and a small portion of its right parietal lobe. For this reason, both the right Asterion and the right Pre-occipital notch landmarks were estimated based on sutures, sulci, and comparing cartesian coordinates of their counterparts on the left side. This specimen was not

rejected because its sulci are some of the clearest among fossil specimen and its mysterious place in human evolution. Visually, the endocranial shape resembles that of Spy 10 with possibly a slight right occipital petalia. Despite the missing parts, the sagittal sinus draining towards the right is clearly visible, as is the dominance of the anterior ramus of the middle meningeal vessels.

3.1.6. *Homo ergaster* (KNMER 3733)

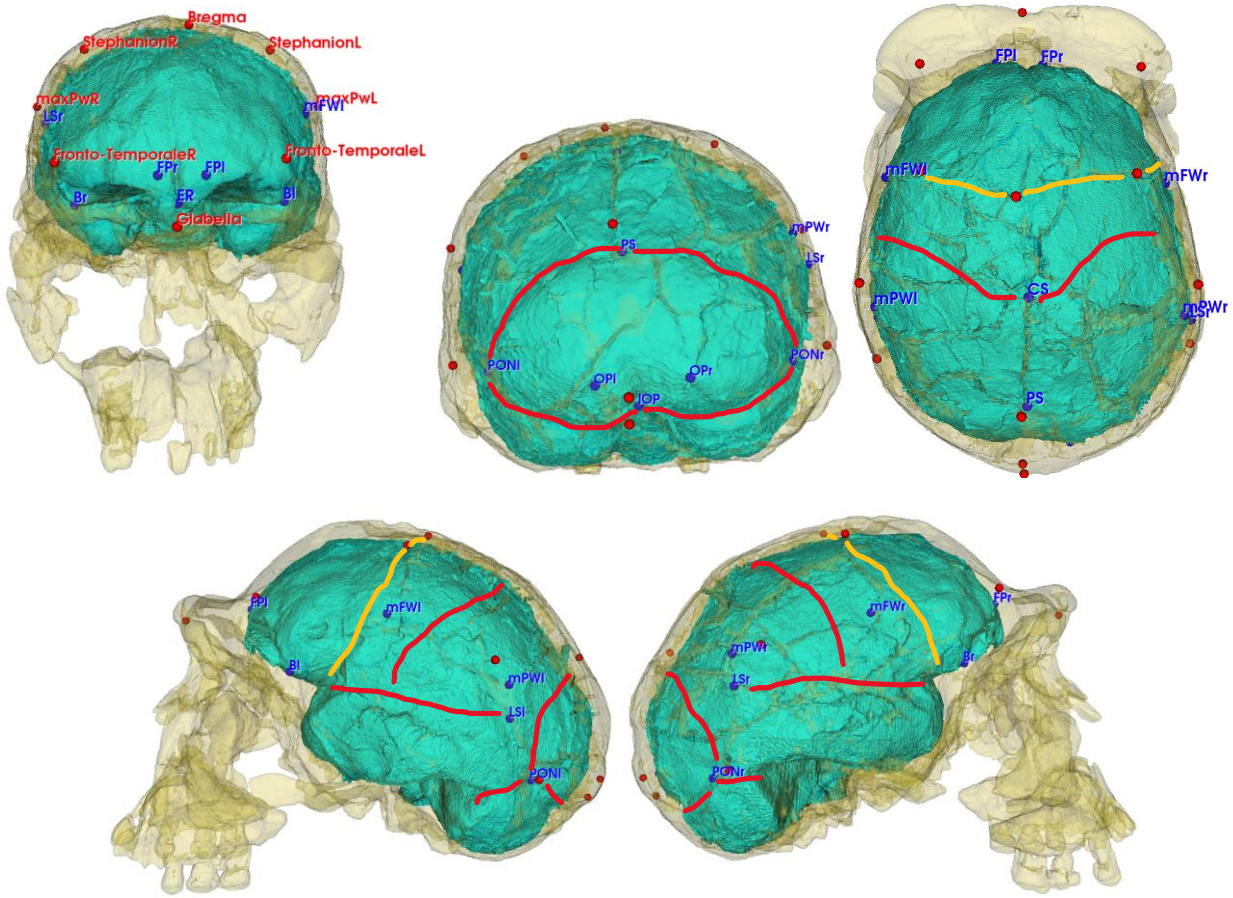

Figure 29: Anterior, Posterior, Superior, and Lateral views of the endocast (cyan, solid) and calvarium (yellow, solid). Endocast landmarks are shown in blue and cranial landmarks in red. Major sulci (red) and coronal suture (yellow).

Homo ergaster is much older than the previous hominins and has quite a different endocast morphology. Apart from being smaller in size, it is widest close to the middle point. The midpoint of the central sulcus also seems to be situated more anteriorly. It is heavily fragmented but well reconstructed and has an overall round shape in the superior view but lacks the cranial vault height of *H. sapiens*. The cranium has heavy

brow ridges. It has a slight left frontal/right occipital petalia, with the sagittal sinus slightly draining rightward and no visible meningeal vessels.

3.1.7. *Homo habilis* (KNMER 1813)

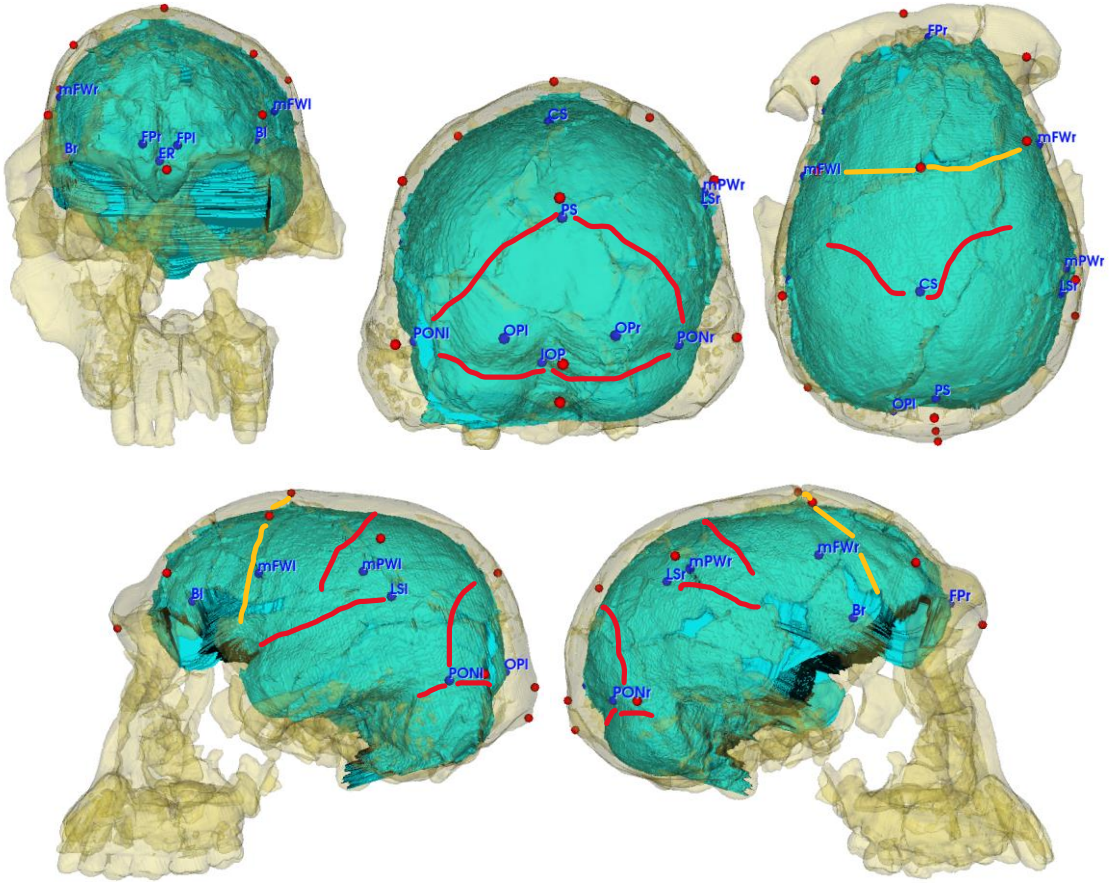

Figure 30: Anterior, Posterior, Superior, and Lateral views of the endocast (cyan, solid) and calvarium (yellow, solid). Endocast landmarks are shown in blue and cranial landmarks in red. Major sulci (red) and coronal suture (yellow).

Compared to the previous specimen, KNMER 1813 has a longer, narrower braincase and more gracile features on the skull. In the occipital and superior view, the right lobes appear more voluminous, and the sagittal sinus drains primarily rightward. It appears smaller in almost every dimension, especially height. Apart from a few areas on the right frontal lobe, the specimen's endocast is well preserved, but difficult to mark with sulci. There are no appreciable traces of the meningeal vessels.

3.1.8. Pan paniscus (Bonobo 27698)

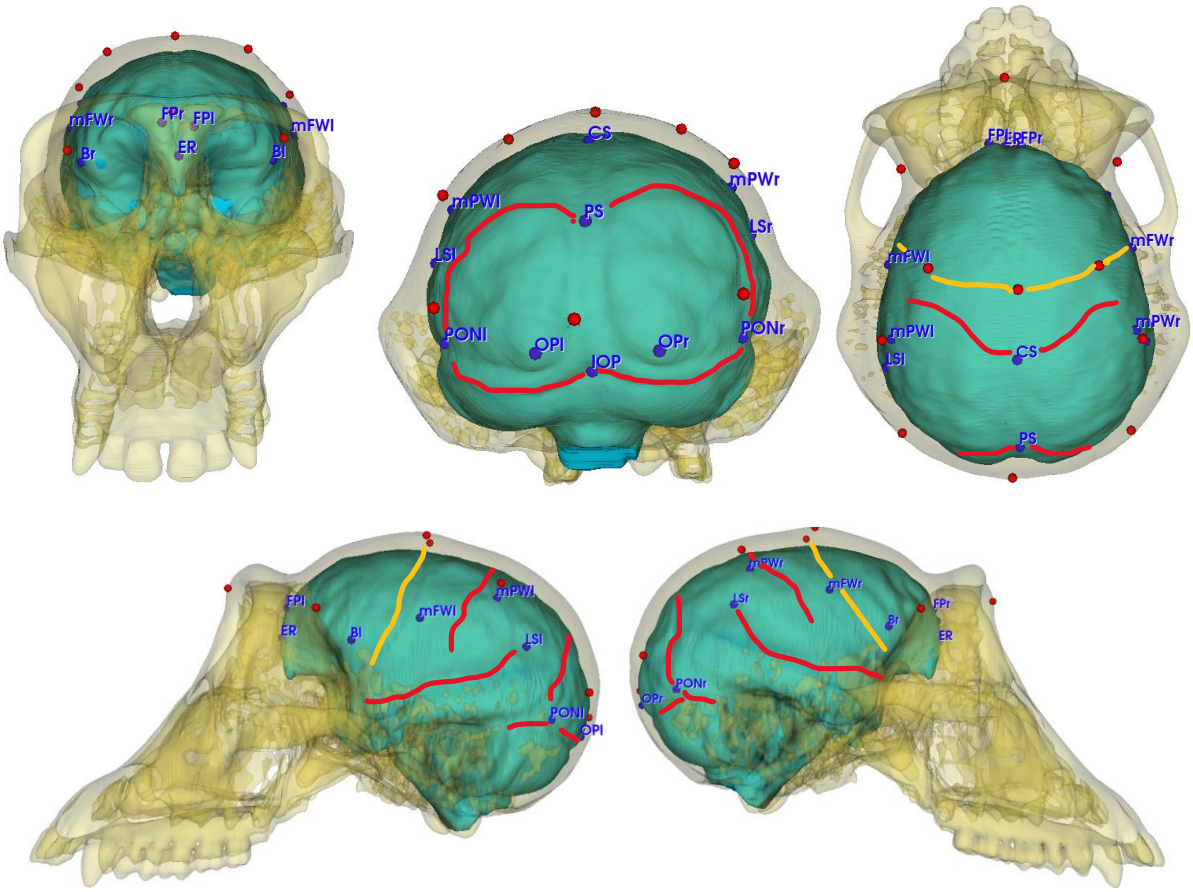

Figure 31: Anterior, Posterior, Superior, and Lateral views of the endocast (cyan, solid) and calvarium (yellow, solid). Endocast landmarks are shown in blue and cranial landmarks in red. Major sulci (red) and coronal suture (yellow).

This is the first specimen outside the genus *Homo*, and it has a visibly distinct cranial morphology with large supra-orbital torus, post-orbital constriction, and robust zygomatic bones. Its endocast is also considerably different from the other specimens, apart from being smaller. It has an ovoid shape, is wide at the base and vertically short. Its frontal lobe is perhaps the most distinct part, as its inferior portion is considerably smaller, to the point that there is an encephalic beak at the anterior most part. This has the consequence of its third frontal convolution being located on the anterior, instead of lateral face. Its maximum parietal width and central sulcus are closer to the center. There are no visible petalias, meningeal vessels, or a preference in the sagittal sinus drainage. Its temporal lobes are also significantly smaller.

3.1.9. Pan troglodytes (Chimpanzee)

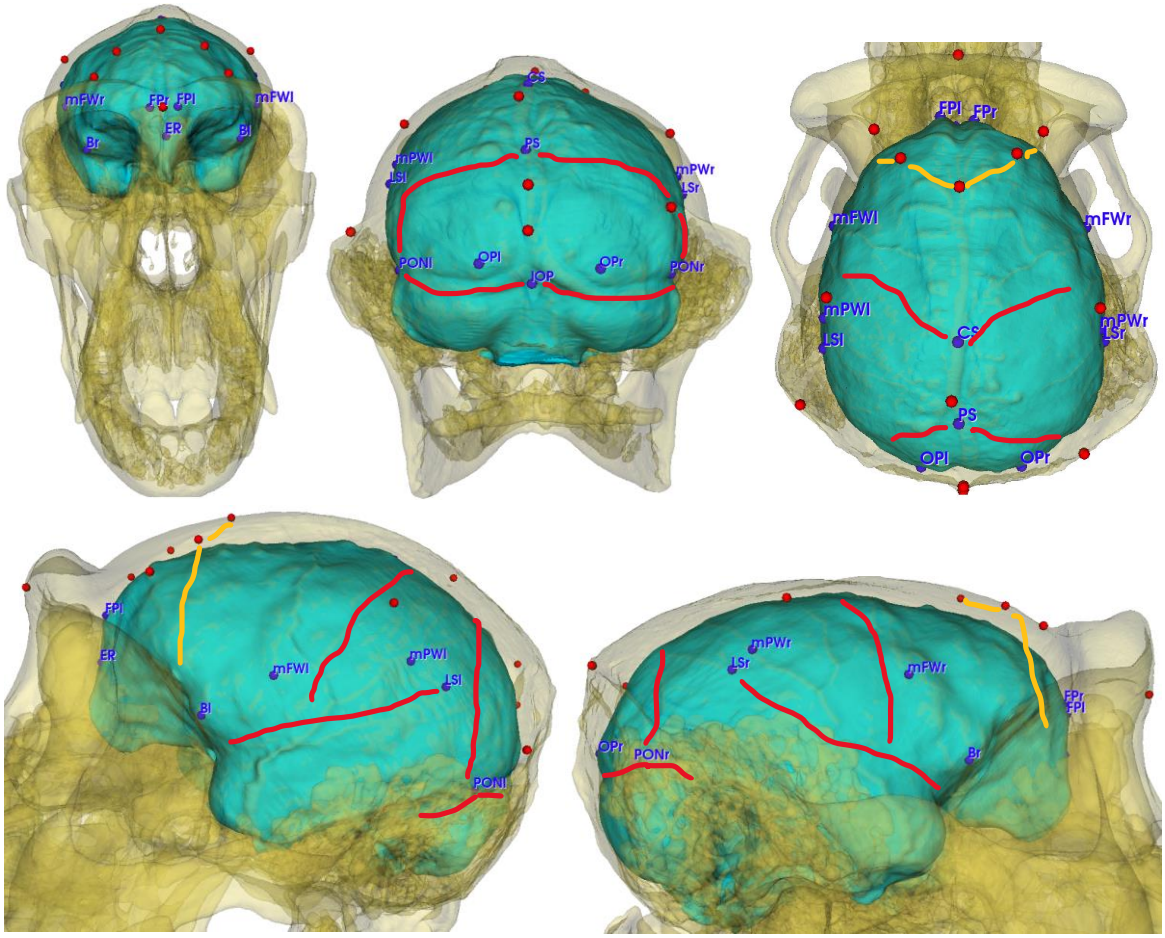

Figure 32: Anterior, Posterior, Superior, and Lateral views of the endocast (cyan, solid) and calvarium (yellow, solid). Endocast landmarks are shown in blue and cranial landmarks in red. Major sulci (red) and coronal suture (yellow).

Perhaps due to sexual dimorphism (this chimpanzee is a male) the brain size relative to its face looks much smaller than that of the bonobo (which was a female). The most visible difference between the two is the space between the coronal suture and the central sulcus. The chimpanzee has the largest distance between the out of all the specimens analyzed so far. Both the chimpanzee and the bonobo have relatively large occipital lobes. The two endocasts are largely alike.

3.1.9. Symphalangus syndactylus (Siamang)

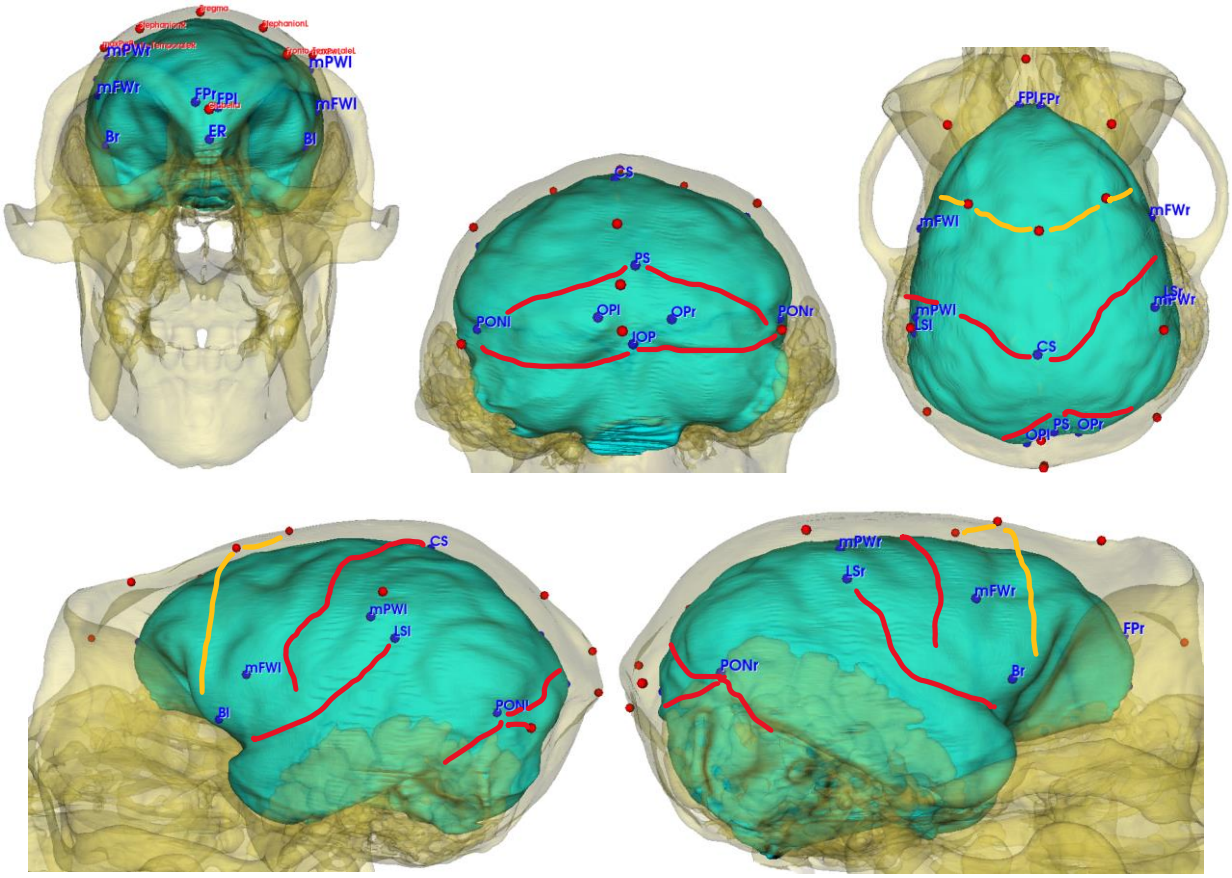

Figure 33: Anterior, Posterior, Superior, and Lateral views of the endocast (cyan, solid) and calvarium (yellow, solid). Endocast landmarks are shown in blue and cranial landmarks in red. Major sulci (red) and coronal suture (yellow).

The siamang is a lesser ape, smaller in body size compared to the *Pan* species. In the superior view, its endocast looks almond shaped, with an even more accentuated reduction in the antero-inferior parts of the frontal lobe. The parieto-occipital and occipital-cerebellar sulci are almost parallel, which is completely different from all other analyzed specimens.

3.1.10. *Mandrillus sphinx*

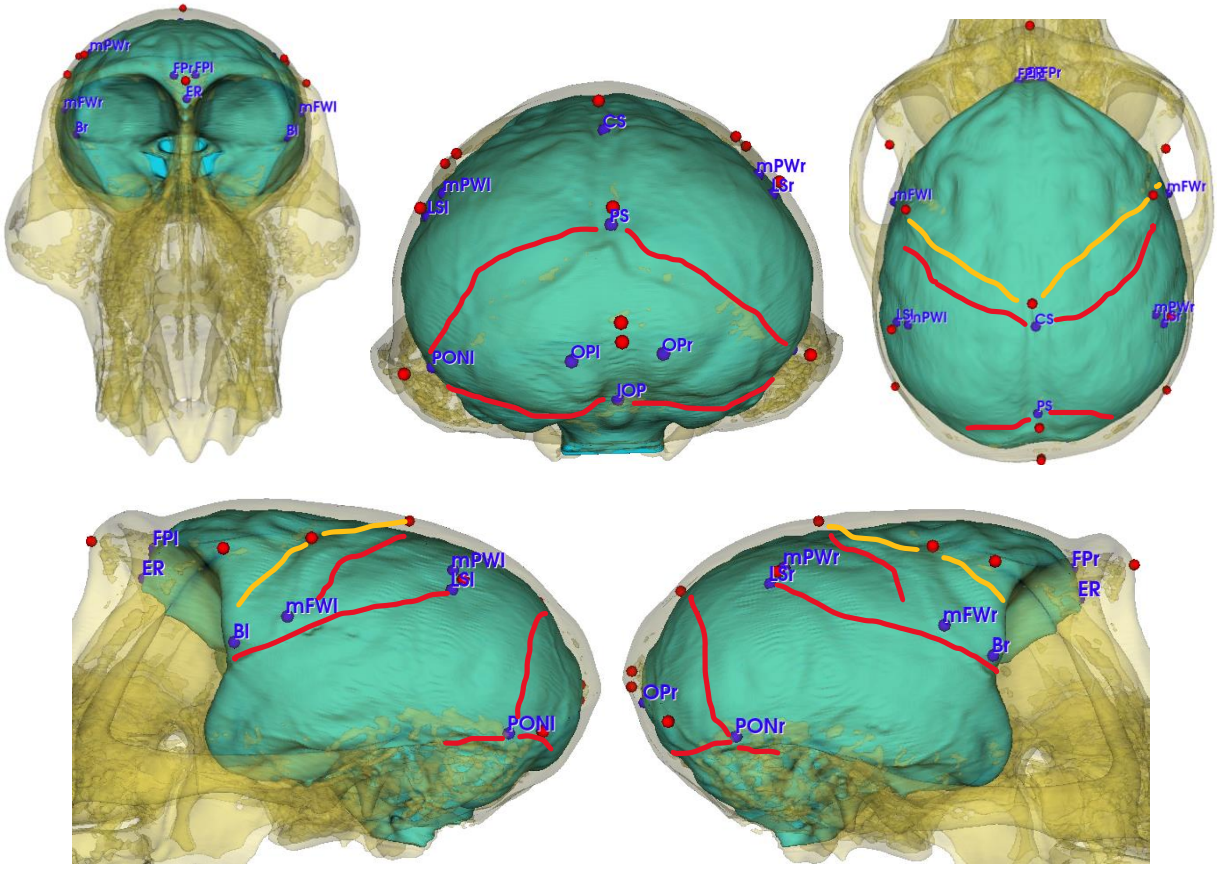

Figure 34: Anterior, Posterior, Superior, and Lateral views of the endocast (cyan, solid) and calvarium (yellow, solid). Endocast landmarks are shown in blue and cranial landmarks in red. Major sulci (red) and coronal suture (yellow).

The mandrill is an Old-World Monkey, and its endocast differs from that of the non-hominin apes in many ways. In the superior view, it resembles the endocast of the siamang. But the frontal poles are noticeably closer. This is in part because of the inferior border of the frontal lobe, which is even higher than those in the *Pan* and the siamang. The third frontal convolution is completely forward-facing and raised superiorly. While the PS and Lambda landmarks are close to each other even in some hominins, the CS and Bregma are never located next to each other, except here. Because the lateral sulci protrude diagonally upwards, they are almost parallel to the coronal suture and the superior part of the central sulcus. The opisthocranion also lies just above the inion, which is unique to this species.

3.1.11. *Papio hamadryas*

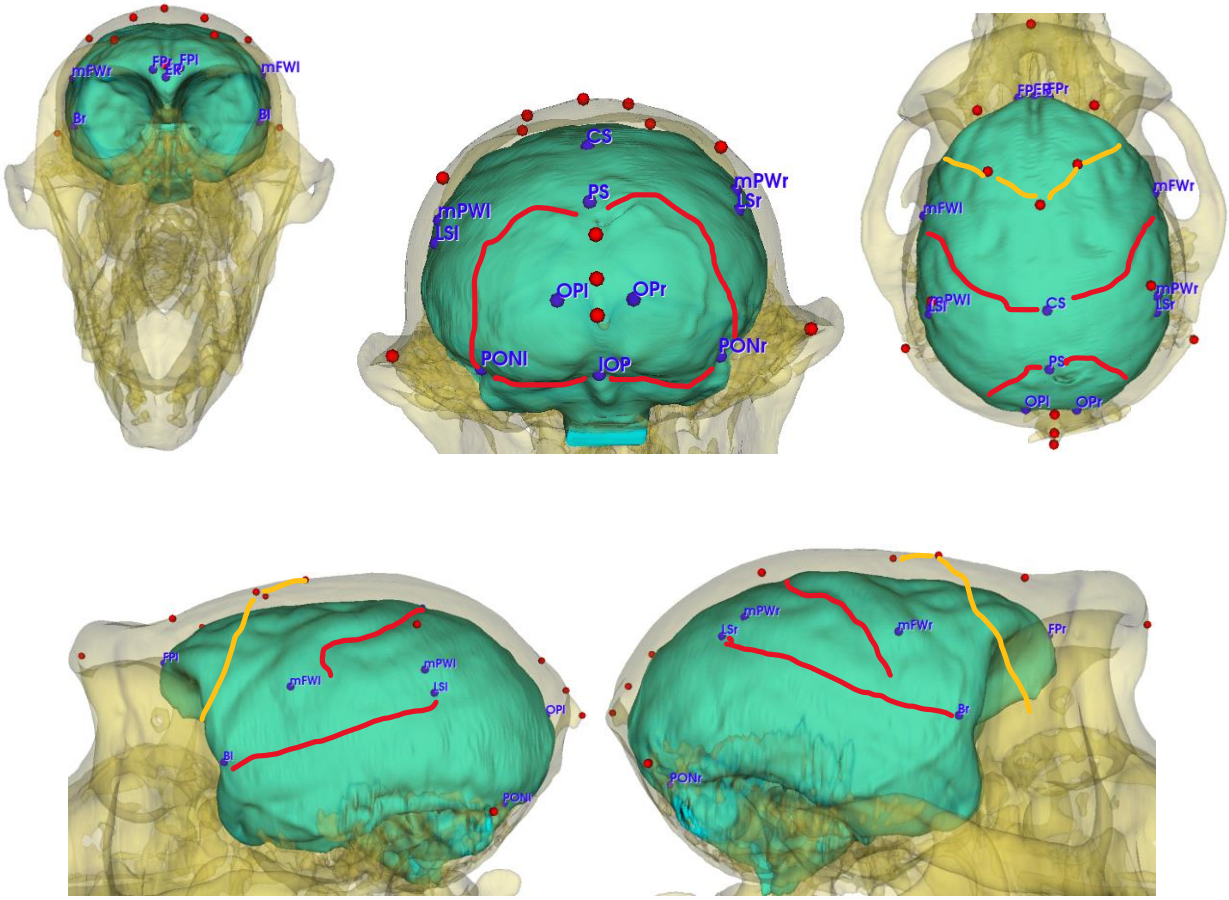

Figure 35: Anterior, Posterior, Superior, and Lateral views of the endocast (cyan, solid) and calvarium (yellow, solid). Endocast landmarks are shown in blue and cranial landmarks in red. Major sulci (red) and coronal suture (yellow).

Baboons are closely related to mandrills, and it can be observed between the two endocasts' overall shape. However, there are a few key differences: the third frontal convolution is located much more inferiorly, the bregma is located more anteriorly, and the opisthocranion is located midway between the lambda and inion, such as in the siamang. Its parieto-occipital sulcus is much more rounded in shape, compared to the almost triangular shaped one of the mandrill.

3.1.12. Macaca arctoides

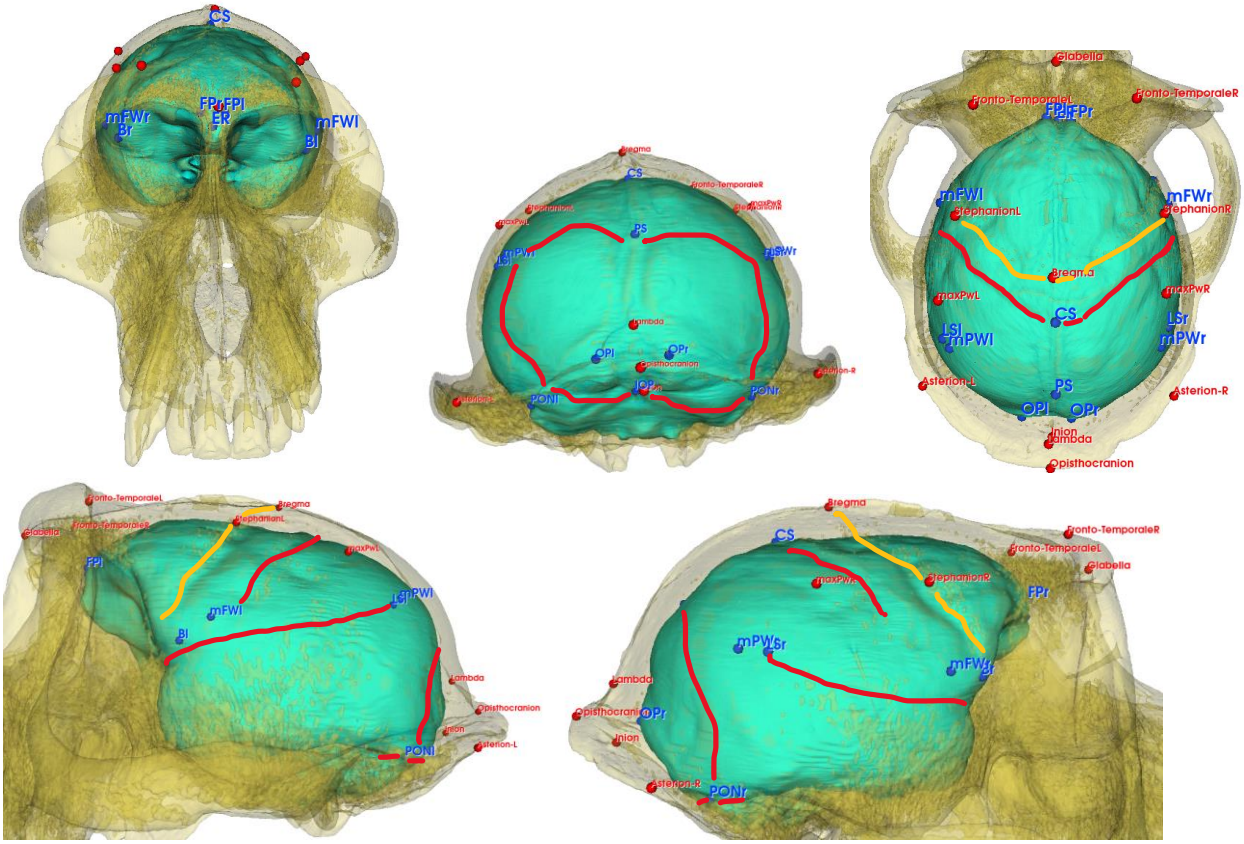

Figure 36: Anterior, Posterior, Superior, and Lateral views of the endocast (cyan, solid) and calvarium (yellow, solid). Endocast landmarks are shown in blue and cranial landmarks in red. Major sulci (red) and coronal suture (yellow).

The Japanese macaque has an almost spherical endocast when observed in the superior view. Like all other Cercopithecoidea in this study, its central sulcus is nearly parallel with the coronal suture, which almost coincides with its precentral sulcus. Its lateral sulci follow the same pattern as the other cercopithecids, proceeding in a linear fashion. Its parieto-occipital sulcus is the most rounded of all cercopithecids. Its bregma is located significantly close to the CS landmark such as in the mandrill, although to a lesser degree.

3.1.13 Alouatta Caraya

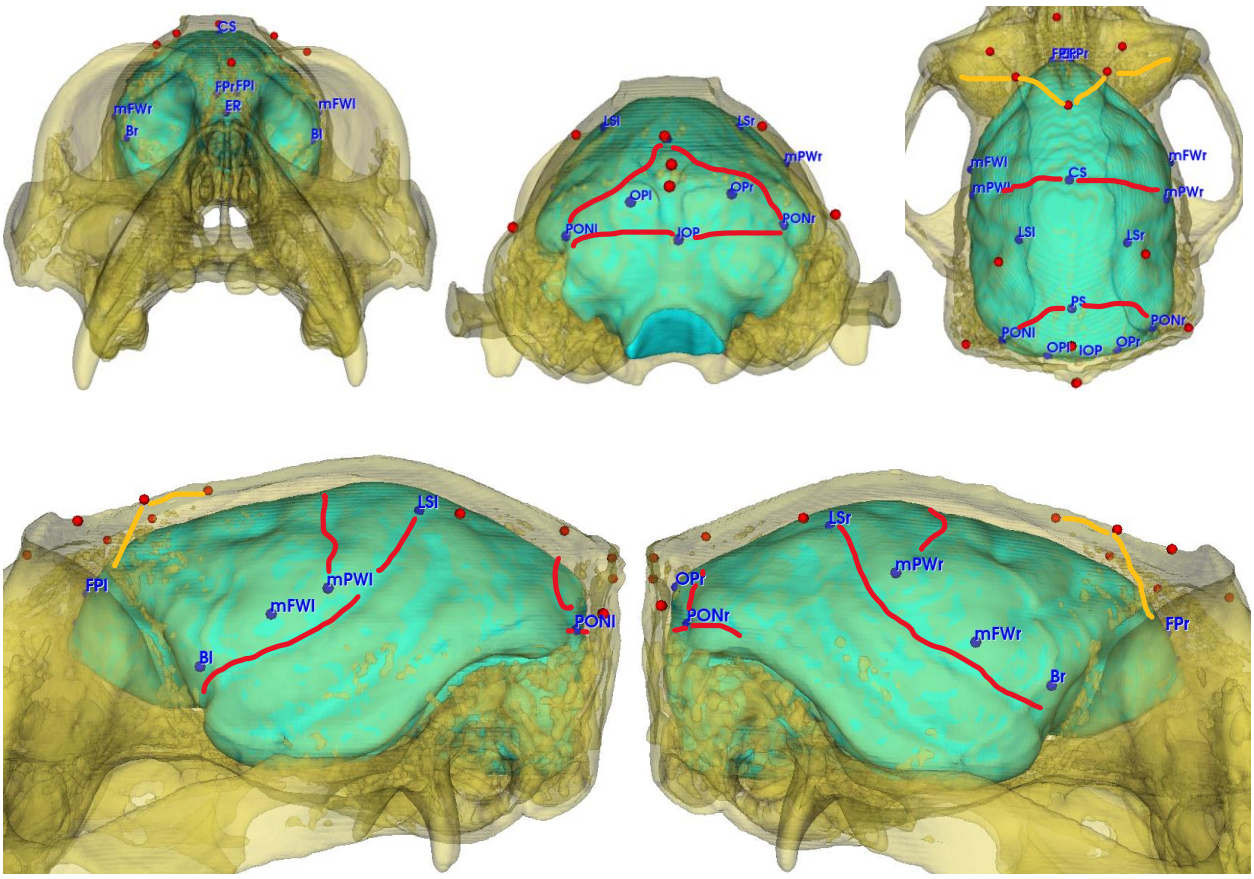

Figure 37: Anterior, Posterior, Superior, and Lateral views of the endocast (cyan, solid) and calvarium (yellow, solid). Endocast landmarks are shown in blue and cranial landmarks in red. Major sulci (red) and coronal suture (yellow).

The only New-World Monkey in this study, the howler monkey, has a completely different overall shape and organization. In the superior view, it has an almost pentagonal shape whereas in the lateral view, the posterior portion of the temporal lobe is visibly constricted. All observable sulci exhibit peculiarities when compared with cercopithecids. The central sulcus travels slightly posteriorly as it proceeds down from the mid-point; the lateral sulcus curves superiorly and travels farther than any other specimen; the parieto-occipital sulcus curves downwards; and the occipital-cerebellar sulcus is almost a straight line. There is also a much larger distance between the CS and PS landmarks.

3.2 Geometric Morphometrics of Endocasts

3.2.1. Mean positions and variability

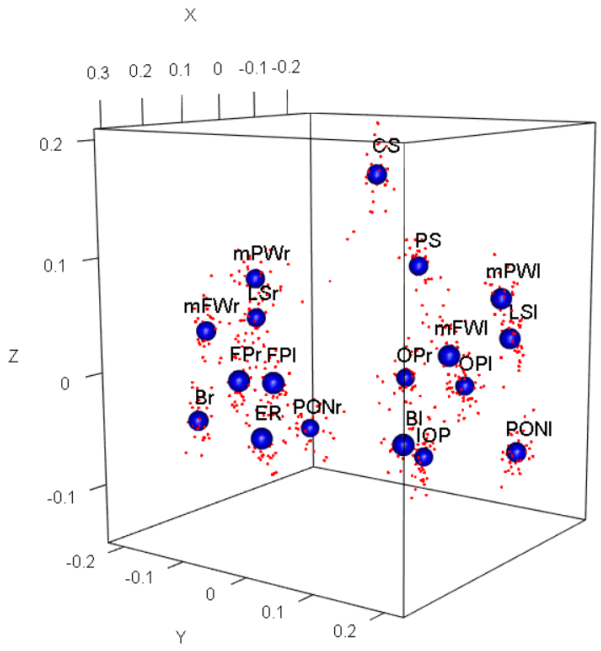

Figure 38: Configurations of landmarks after GPA (in red) and the mean config. (in blue).

Landmark	StdDev
LSl	0.06346153
LSr	0.06087215
mPWr	0.05829140
mPWl	0.05762342
CS	0.05634784
PONl	0.05448948
PONr	0.05205443
ER	0.04700543
mFWr	0.04698824
mFWl	0.04522033
IOP	0.04431406
PS	0.04305624
Bl	0.04082991
OPl	0.04058631
Br	0.04009098
OPr	0.03897817
FPl	0.03535952
FPr	0.03467397

Figure 39: Landmarks and their standard deviations after GPA.

The first 7 landmarks with the greatest amount of variation correspond to the parietal lobe and its borders. While it could truly mean that this region shows the greatest amount of variation in the sample, a few people have already noted difficulties in accurately determining the locations of landmarks here (Maudgil et al. 1998; Bienvenu et al., 2011). However, errors on simple landmarks such as the maximum parietal widths are less likely, and almost certainly suggest a high variability across this sample. Because the LS landmarks are generally located close to the mPW landmarks, it is likely that the high variability is not a result of errors in landmarking. It is also unlikely that the PON landmarks are erroneously marked, as they are one of the easiest landmarks, being well-delimited in almost every endocast by the occipital-cerebellum sulci.

On the other hand, low variability across the lengthwise extremes of the specimens, i.e. the frontal and occipital poles, and the third frontal convolutions is observed.

3.2.2. Principal Component Analysis

3.2.2.1. PC1 vs PC3

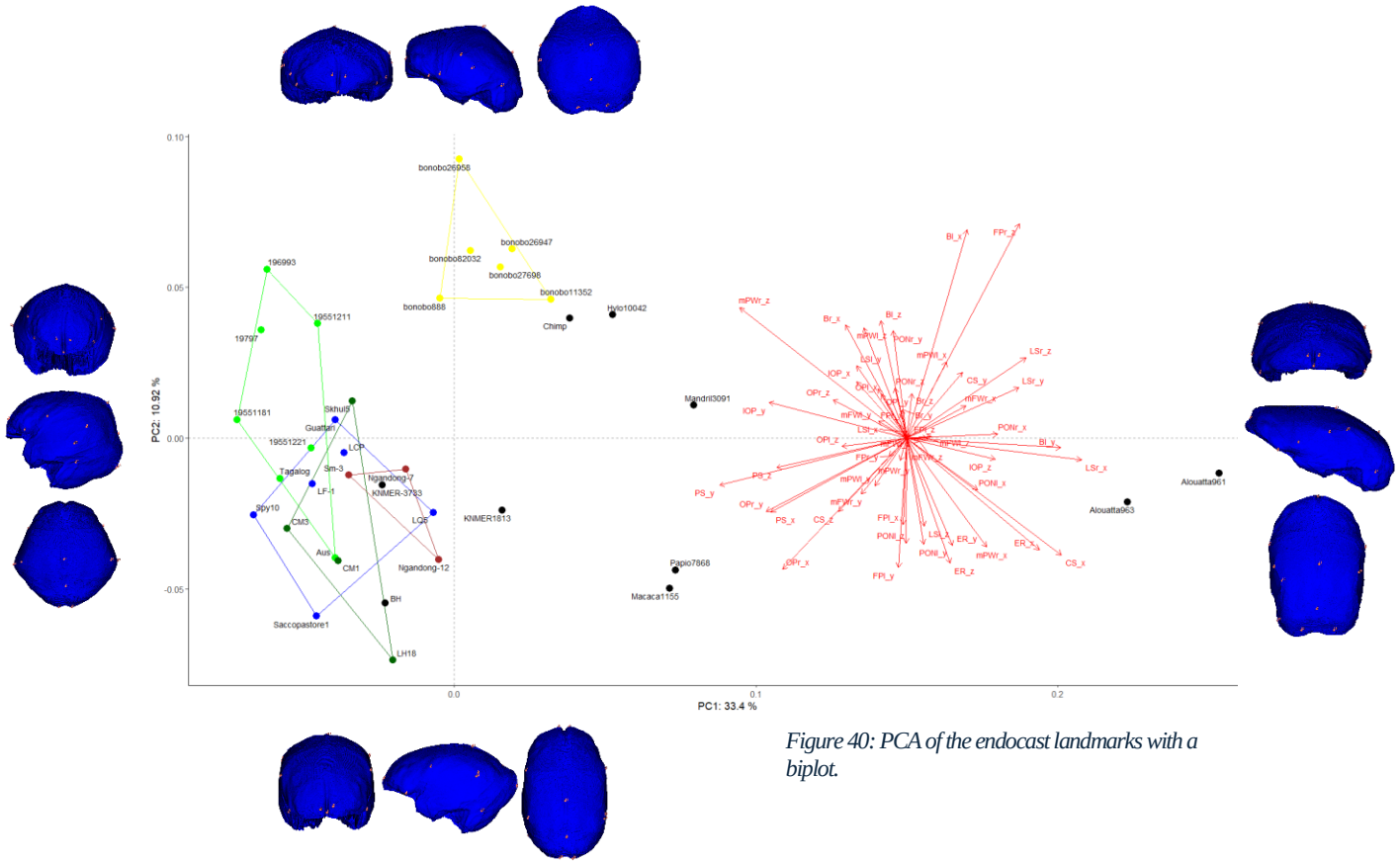

Figure 40: PCA of the endocast landmarks with a biplot.

The specimens have clustered appreciably, considering the reported ambiguities with these landmarks. The first 2 PCs explain a total of ~ 44% variance. PC1 (positive direction) mainly concerns the antero-inferior retrusion of the PS, the lateral protrusion of LS, antero-superior extension of the frontal lobe as well as a widening at the third convolution, and a lateral separation of the occipital poles. These are the most striking differences of the howler monkeys from *Homo*, and they are hence placed farthest along this axis, with the mandrill intermediate in position between the two, close to the axis.

The macaque and baboon are placed close to each other and differ most from prehistoric *Homo* because of their relatively lesser lateral (at LS) and superior (at CS) projection, and overall lesser curvature on

the superior surface. Interestingly, *Homo habilis* sits in between the two groups, while being much closer to *Homo*.

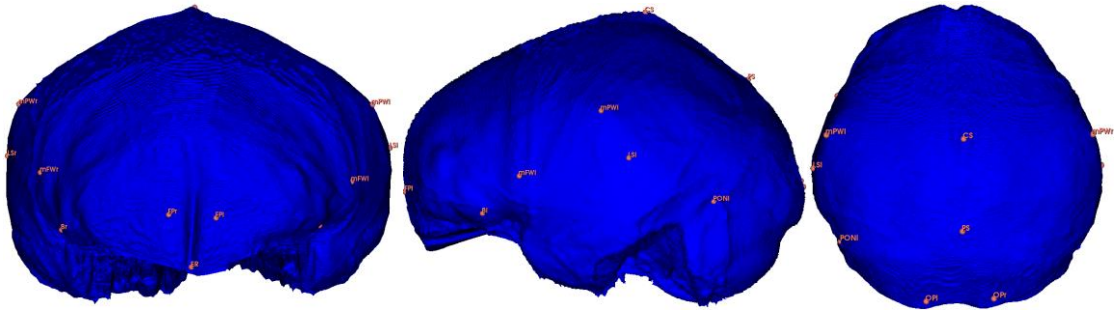

Figure 41: Approximate morphed configuration of the bonobo average.

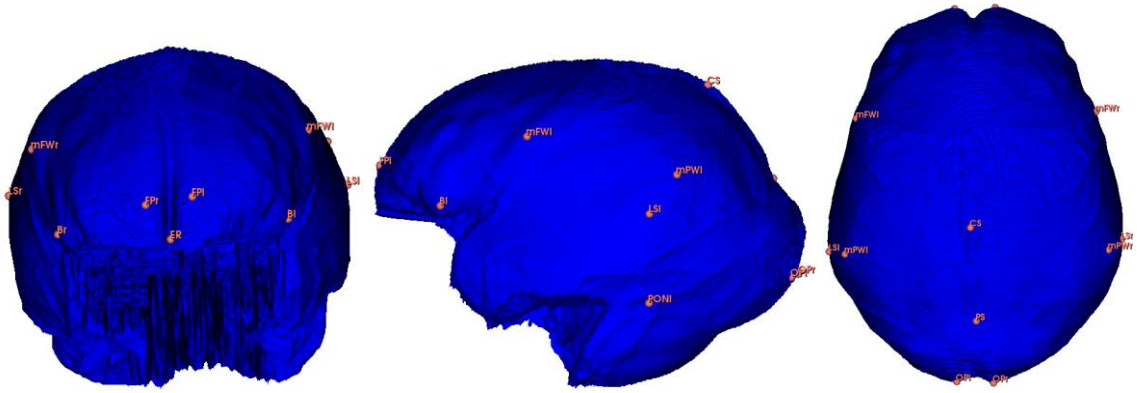

Figure 42: Approximate morphed configuration of the prehistoric Homo average.

Bonobos, the chimpanzee, and the siamang are situated far away from *Homo*, differing mostly by a more inferiorly placed frontal lobe, maximum lateral width being situated more anteriorly, wider lobes, and a counterclockwise rotation of the parietal landmarks.

Within *Homo*, there is a significant overlap. The modern humans are most divergent, differing from the fossil specimens mostly along PC2, like bonobos, except that they slightly decrease in value along PC1 whereas bonobos considerably increase. Therefore, apart from the differences that they share with bonobos from fossil *Homo*, they also have a slightly higher cranial vault.

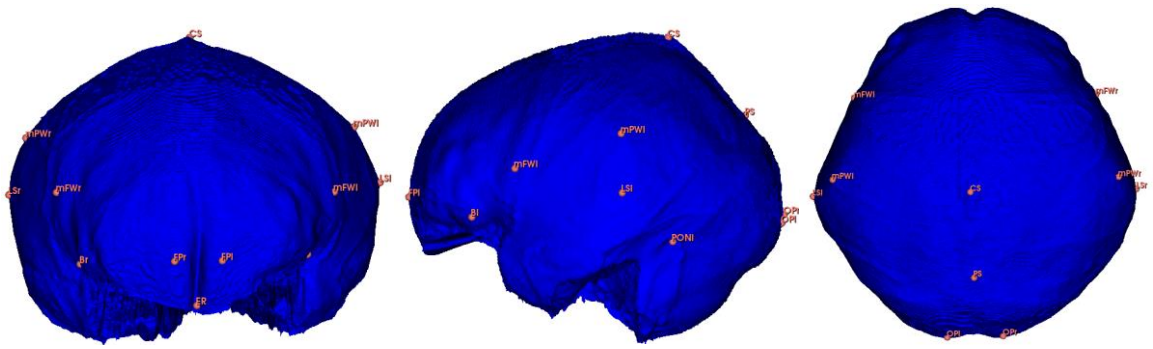

Figure 43: Approximate morphed configuration of the prehistoric Homo average.

Within prehistoric *Homo*, it is difficult to distinguish between the models. Broken hill is placed on the convex hull of Pleistocene *H. sapiens* but this may not mean much due to the deformed nature of LH18. In either case, it is laterally narrower and anteroposteriorly longer, vertically flatter, and its superior surface being less curved than the other Pleistocene *H. sapiens*. The *Homo erectus* specimens are on average, vertically flatter, laterally narrower, and have a less curved superior face when compared to Pleistocene *H. sapiens*. KNMER 3733 (*Homo ergaster*) interestingly falls inside the variation of *Homo erectus*.

The largest overlap is between Pleistocene sapiens and Neanderthals, with the latter group having more variation along PC2, but perhaps this is because of the greater number of samples. This is overcome by using PC3.

3.2.2.2. PC1 vs PC3

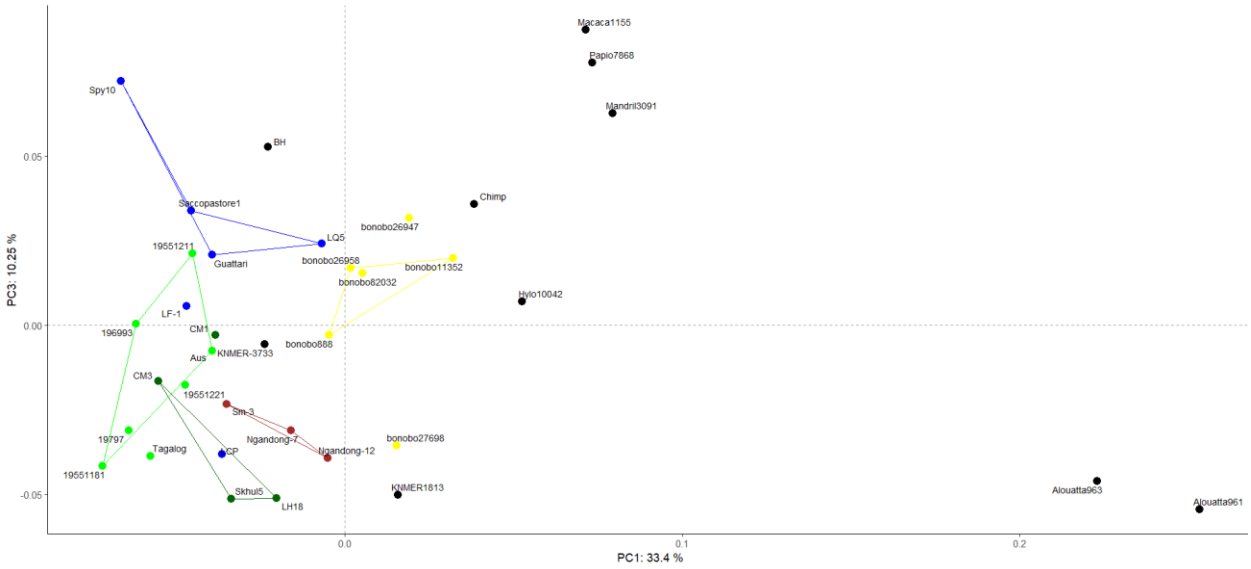

Figure 44: PC1 vs PC3

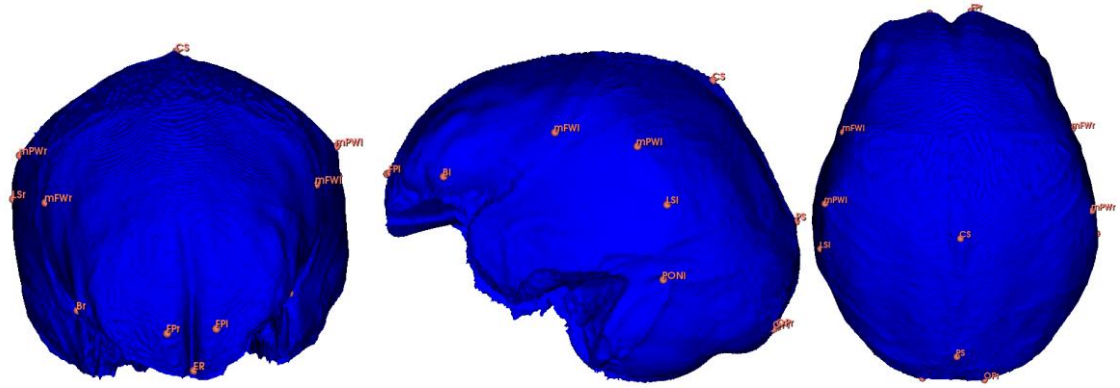

Figure 45: Approximate morphed configuration of the Prehistoric H. sapiens average.

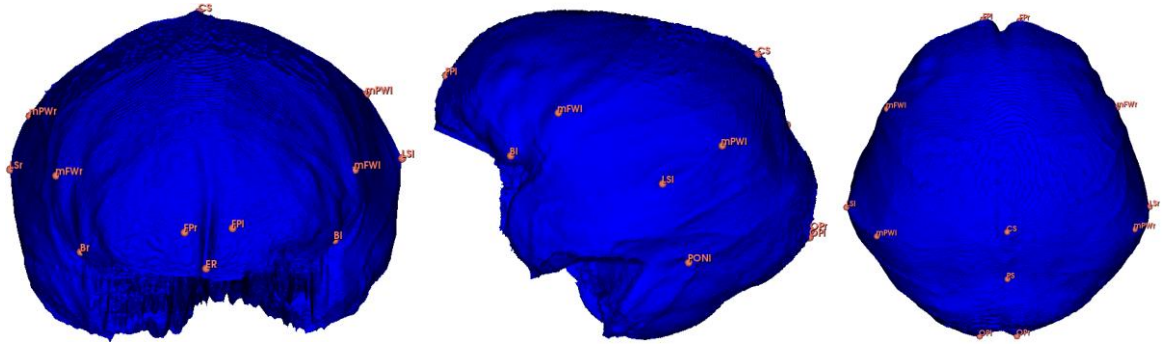

Figure 46: Approximate morphed configuration of the Neanderthal average (excluding LCP).

Neanderthals and BH can be largely distinguished from *H. sapiens* through their relatively higher and posteriorly tilted frontal lobes, antero-laterally positioned LS, anteriorly positioned PS, and a more posteriorly positioned maximum parietal widths. However, LF1 falls within the variation of modern humans, and LCP within prehistoric *H. sapiens*.

KNMER 3733 lies intermediate between Neanderthals and *H. erectus* along PC3, while KNMER 1813 lies at the same level as fossil *H. sapiens*.

Homo erectus can be distinguished from Pleistocene *H. sapiens* because of their higher frontal and occipital extremities (including the PS) and vertically flatter shape.

3.3. PCA of Euclidean Distances Between Endocast and Calvaria Landmarks

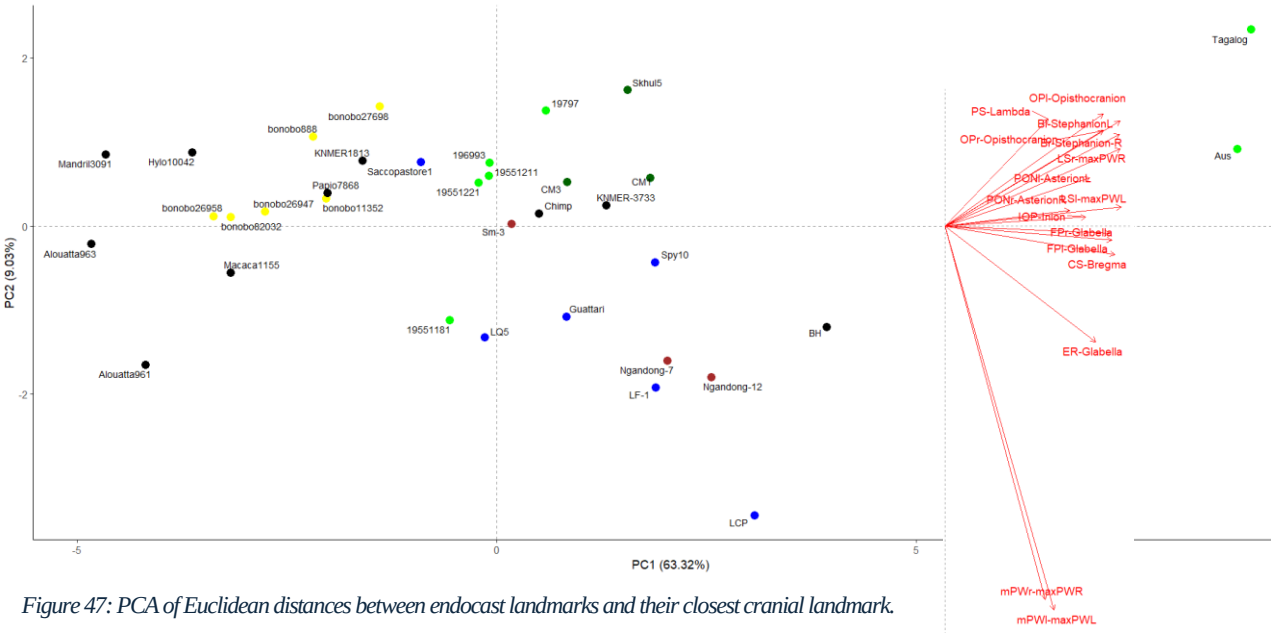

Figure 47: PCA of Euclidean distances between endocast landmarks and their closest cranial landmark.

The two PCs contribute to more than 72% of the total variance. There is a clear distinction, with most hominins on the right side of PC1 and most non-hominins on the left, with the curious exceptions of *Homo habilis* and the chimpanzee.

The Tagalog and Australian specimens are the outliers, with the highest LS-maxPW distances distinguishing them from other *H. sapiens*.

Distance	Standard Deviation
LSr-maxPWR	51.402103
LSI-maxPWL	29.936499
CS-Bregma	22.184449
Br-Stephanion-R	19.681567
BI-StephanionL	17.900567
PONr-AsterionR	11.109287
OPI-Opisthocranion	10.052767
PONI-AsterionL	9.517454
OPr-Opisthocranion	8.451936
FPI-Glabella	8.316044
ER-Glabella	7.478944
FPr-Glabella	7.426696
IOP-Inion	7.369520
mPWI-maxPWL	6.606651
mPWr-maxPWR	5.864518
PS-Lambda	5.232892

Figure 50: Standard deviations of Euclidean distances.

	ID	Procrustes Distance
2	Sm-3-endo	0.0648897
3	Aus-endo	0.0778019
4	Ngandong-7-endo	0.0837497
5	19551211-endo	0.0866119
6	LCP-endo	0.0873471
7	bonobo26947-endo	0.0885597

Figure 49: Procrustes distances for Endocast-only landmark GPA.

H. sapiens – prehistoric and modern cluster fairly close to each other, being distinguished mainly by the FP-Glabella distances, along with IOP-inion, and CS-Bregma (lesser in modern humans). Together, they can be distinguished from all other archaic hominins mainly by a much lower ER-Glabella, and distances between the points of maximum parietal widths.

On the other side of the morphospace, the howler monkeys also are most affected by occipital lobe distances, and that of the Broca-Stephanion.

Interestingly, Sm-3 ended up almost at the origin of the morphospace, while also having the least Procrustes distances in the GPA with endocast landmarks.

Broken Hill is situated close to the Neanderthals and *H. erectus*, with larger frontal, and IOP-Inion distances.

Overall, the frontal and parietal width distances seem to be the most distinguishing distances between hominins.

4. Discussion and Conclusion

This study has provided a brief overview of the shape and organization of endocasts. It has also used virtual anthropological methods to quantify and visualize the greatest variations between these, based on landmarks that have been questioned. Based on the degree of clustering in the PCA plots (both with cranial landmarks and without), it can be said that these landmarks are capable of distinguishing specimens at the very least on the genus level. It would be interesting to use more extant specimens belonging to the same genus but different species, to further test their viability.

On the qualitative side, the extant apes and monkeys did not present a single case of a petalia or meningeal vessels, although there were a few that had asymmetric sagittal sinus drainage. The sagittal sinuses itself was faint on the monkeys, except at the anterior and posterior ends.

The placement of landmarks and marking of sulci was undertaken multiple times on the same models over the last few months, each time after consulting more information on brain anatomy. This led to the realization of the factors that influence sulci detection: expertise, intra-observer error, apart from those dependent on the 3D models. The most difficult, and hence least reliable landmark, was the CS. LS was challenging at times as well, confirming (Labra et al., 2024). It was, however, much easier to place landmarks on specimens the further they got phylogenetically to hominins. This may be because there are fewer convolutions in total. It is probably not because of good preservation (because they are extant) as extant humans were extremely challenging to landmark.

Lastly, it has been shown through the landmark-distance study that extinct Homo and extant simiiformes have a degree of correspondence between their endocast and calvaria that is mostly consistent with their phylogenetic relationships. However, the relationships are not strong enough at the moment to be able to predict the position of endocast landmarks through cranial landmarks, and perhaps never may be as

there are great differences across specimens and species. The Tagalog and Australian specimens clustering far away from other specimens was surprising and may have something to do with their imaging as they belong to the same collection.

Although the reliability of the landmarks on the endocast can never truly be tested in the absence of living hominins, they enable the quantification of shape and organization of the only tangible proxies of brains. This study has demonstrated that analysis of crania and endocasts together to quantify differences and establish relationships across specimens holds great potential. The obvious next step would be to include more specimens, both extant and extinct.

Bibliography

Albessard, L. (2018). Morphological Covariation of the Skull and Endocranium during the Evolution of the genus Homo.

Balzeau, A., & Mangin, J.-F. (2021). What Are the Synergies between Paleoanthropology and Brain Imaging? Symmetry, 13(10), Article 10. https://doi.org/10.3390/sym13101974

Bruner, E., Ogihara, N., & Tanabe, H. C. (Eds.). (2018). Digital Endocasts. Springer Japan. https://doi.org/10.1007/978-4-431-56582-6

Dumoncel, J., Subsol, G., Durrleman, S., Bertrand, A., de Jager, E., Oettlé, A. C., Lockhat, Z., Suleman, F. E., & Beaudet, A. (2021). Are endocasts reliable proxies for brains? A 3D quantitative comparison of the extant human brain and endocast. Journal of Anatomy, 238(2), 480–488. https://doi.org/10.1111/joa.13318

Grimaud-Herve, D., & Holloway, R. L. (n.d.). SPY I AND SPY II CRANIA AND MANDIBLES. ENDOCASTS.

Ponce de León, M. S., Bienvenu, T., Marom, A., Engel, S., Tafforeau, P., Alatorre Warren, J. L., Lordkipanidze, D., Kurniawan, I., Murti, D. B., Suriyanto, R. A., Koesbardiati, T., & Zollikofer, C. P. E.

(2021). The primitive brain of early Homo. Science, 372(6538), 165–171. https://doi.org/10.1126/science.aaz0032

M.A. Willis, D.E. Haines, in Fundamental Neuroscience for Basic and Clinical Applications (Fifth Edition), 2018

https://www.hopkinsmedicine.org/health/conditions-and-diseases/anatomy-of-the-brain

https://www.science.org/doi/10.1126/science.aba1135

https://upload.wikimedia.org/wikiversity/en/8/82/Medical_gallery_of_Blausen_Medical_2014.pdf

https://www.ncbi.nlm.nih.gov/books/NBK538496/

https://www.britannica.com/science/human-nervous-system/The-central-nervous-system